Renewable Energy 145 (2020) 242–260

Contents lists available at ScienceDirect

Renewable Energy

journal homepage: www.elsevier.com/locate/renene

Mechanical analysis of photovoltaic panels with various boundary condition

Yongxue Li [a], Lingzhi Xie [a, b, *], Tengyuan Zhang [b], Yupeng Wu [c], Yanyi Sun [c], Zhichun Ni [d], Jingquan Zhang [e], Bo He [b], Peng Zhao [a]

[a] College of Architecture and Environment, Sichuan University, Chengdu, 610065, PR China
[b] Institute of New Energy and Low-carbon Technology, Sichuan University, Chengdu, 610207, PR China
[c] Department of Architecture and Built Environment, Faculty of Engineering, University of Nottingham, University Park, Nottingham NG7 2RD, UK
[d] Suzhou Talesun Solar Technologies Co., Ltd., Chang Shu, 215542, PR China
[e] College of Materials Science and Engineering, Sichuan University, Chengdu, 610065, PR China

ARTICLE INFO

Article history:
Received 26 December 2018
Received in revised form
25 May 2019
Accepted 28 May 2019
Available online 31 May 2019

Keywords:
Photovoltaic panel
Various boundary condition
Classical lamination theory
Rayleigh-Rita method
Modified deflection function
Bending experiment

ABSTRACT

The photovoltaic (PV) panels currently existed on market are laminated plate structures, which are composed of two stiff glass skins and a soft interlayer. Some panels are installed on the buildings and integrated as the components of the structures, such as wall and roof. In different locations, the installations of PV panels are different and the boundary conditions are not always simply supported. In this paper, the bending behaviour of PV panels with various boundary conditions is analysed and the influence of boundary condition is studied carefully. The Kirchhoff theory is adopted to build governing equations of PV panels under static force. A Rayleigh-Rita method is modified to solve the governing equations and calculate the static deformation and stress. Different boundary conditions usually require different assumptions of the deflection function, but a modified general function is developed in here to solve that problem. A theoretical solution is derived out and used to do the numerical calculation. The bending experiments of PV panels with two boundary conditions are used to verify the accuracy of the proposed solutions. Finally, the influence of different boundary condition is stated by comparing the numerical results and some guides for the PV panel installation are proposed.

1. Introduction

In a report from China Association of Building Energy Efficiency, it consumes 40%–50% of the total energy each year in building structures in P.R. China [1]. It's almost the same in U.S. since U.S. Department of Energy stated that building consumes more than 40% of the electricity produced in U.S. every year [2]. The huge demand of energy brings plenty of non-renewable and non-recyclable wastes. Meanwhile, several green and renewable energies are developed fast in recent decades, such as solar energy, wind energy and geothermal energy. If those green energies could be utilized in the building, the energy consumption could be reduced and less wastes will be made to the environment. One of those tries is building integrated photovoltaic (BIPV), which has attracted much attention from the engineers and researchers. Different from traditional building attached photovoltaic (BAPV) technology, the photovoltaic (PV) module in BIPV must be a functional part of the building. It requires that the PV component must generate electricity for the building to reduce the energy needs, and at the same time, to bear external loads and keep the safety and integrality of the building.

In 1970s, it is the first time for PV modules to be applied in civil engineering and they were usually mounted on buildings skin, which is just BAPV [3]. Two decades later and in 1990s, PV module started to be integrated into building, and some relative research works were promoted [3,4]. In several review papers [4–9], the history, development and future opportunities of BIPV are stated carefully. However, it denotes that the mechanical behaviour of the BIPV products are studied much less than energy efficiency [10], thermal behaviour [11–13] and other properties [14,15]. Peng etc. [16] pointed out that the building loads and PV module damages should be considered in design work.

* Corresponding author. College of Architecture and Environment, Sichuan University, Institute of New Energy and Low-carbon Technology, Sichuan University, No. 24 South Section 1, Yihuan Road, Chengdu, 610207, PR China.
E-mail address: xielingzhi@scu.edu.cn (L. Xie).

https://doi.org/10.1016/j.renene.2019.05.121
0960-1481/

There are several different types of PV modules in the commercial market right now, including monocrystalline silicon module, polycrystalline silicon module, cadmium telluride module, Cu indium gallium selenide module and amorphous silicon module. All of them utilize glass to be the cover plate since the sunlight must be transmitted though the cover plate to PV cell layer. But the bottom plate has different choices. The single glass PV module uses opaque TPT and double glass PV module adopts the transparent glass. In BIPV, the double glass PV module with better photo-permeability are more suitable and acceptable in the real structures. Therefore, the PV panels studied in the present paper are double glass PV panel which consists of two glasses and an interlayer in where the cells are sealed by ethylene vinyl acetate (EVA) or polyvinyl butyral (PVB).

Among the requirements to double glass PV panels in BIPV, generating electricity is the nature function and all the normal commercial products could satisfy that requirement. Therefore, the difficult problem is whether those PV panels are qualified as the building component to bear different external loads. Until now, only in the standards of PV module itself, such as IEC 61215 (2005) [17], there are several codes about the mechanical properties and the corresponding test methods [4]. It is lack of specific codes about PV modules applied in BIPV. As to the mechanical analysis, the main of them are just bending behaviour and impact behaviour, which represent the static property and dynamic property, respectively. In the present paper, it focuses on the bending behaviour of double glass PV panels, and it can supply the foundation to the further safety research and design codes of PV panel under wind load or snow load in buildings.

In studies about bending behaviour of double glass PV panel, Naumenko and Eremeyev [18] used layer-wise theory and they treated the PV panel as a layered composite with two relatively stiff skin layers and a relatively soft core, since the ratio of shear moduli $\mu = G_c/G_s$ for core material to skin glass is in the range between 10^{-5} and 10^{-2}. But only the plate strip with simply supported boundary condition is solved in their paper. Eisentrager etc. [19] presented a finite element formulation and a user-defined quadrilateral serendipity element with quadratic shape functions and nine degrees of freedom. They are based on layer-wise theory and used to analyze the bending behaviour of PV module with two boundary conditions. Eisentrager etc. [20] also tried another method, first order shear deformation theories (FSDT), to study the PV panel with weak shear stiffness. They developed a user-defined element and integrate it into ABAQUS. Weps [21] chose unsymmetrical laminated beam to study and they used layer-wise theory to build the constitutive equations. The proposed equations and finite element analysis are verified by the three-point bending test. Besides, symmetrical laminated glass beam for PV application were completed by Schulze etc. [22]. They firstly simulate PV module as laminated structure with relatively soft core. In the authors' previous work [23], the double glass PV panel with a special boundary condition, two opposite edges simply supported and the other two edges free, is studied theoretically and experimentally. Hoff model is adopted to simulate the panel, and Rayleigh-Rita method is modified to obtain static deformation. But the influence of boundary condition is not discussed carefully, and the differences between proposed method and classical method are not stated.

Since double glass PV panel is actually a laminate composite, the theories and mechanic models of that composite could be applied in this research. Vedrtnam and Pawar [24] made a review work on laminate composite, and laminate glass plate which is very like double glass PV panel is mainly introduced. First order shear deformation theory (FSDT) is a theory for laminate composite, and the principle assumption of it is that the normal variables to the middle surface of plate behave like rigid bodies during the bending test. Those variables are defined as constants, including displacement and transverse shear stress. Based on FSDT, some analytical or semi-analytical solution are derived out and verified by experiments or simulations [25–31]. Zig-zag theory utilizes the piecewise functions to describe displacements of the plate with respect to the thickness coordinate, and the governing equations can be simplified [32–35]. Layer-wise theory (LWT) was chosen by many researchers to study PV panel. In LWT, the constitutive equations are derived out for each layer, and interaction forces and compatibility are calculated by some specific models [18,19,21,36–41]. Some other theories and models were also proposed, such as trigonometric shear deformation theory [42], new higher order shear deformation theory [43,44], and so on. In addition, other researchers did some works on the methods to solve the partial differential equations and obtain the final solutions, including closed-form solutions or approximate analytical solutions [45–47]. However, in many of those works, the boundary conditions of the plates are four edges simply-supported since it is easy to get solutions. And there are very few works discussing the influence of different boundary conditions.

Actually, the installation ways of double glass PV panel on the steel frame are very different in the buildings, including four edges simply supported, two opposite edges simply supported and the other two edges free, and four points supported. Different installation ways mean different boundary conditions to the PV panel, and the mechanical behaviours are also different. It is necessary to do some studies on the influences of boundary condition, so it will be helpful to the design and running of double glass PV panel when it is applied in BIPV.

In present paper, the mechanical properties of double glass PV panel with two different boundary conditions are analysed by both experimental and theoretical researches. A classical lamination theory, Hoff model, is applied to build the constitutive equations of whole panel under the uniformly distributed force. The specific boundary equations are given based on two boundary conditions: four edges are simply supported (annotated as SSSS), two opposite edge are simply supported and the other two edges are free (annotated as SSFF). The Rayleigh-Riata method is modified to derive the closed form solution. Although boundary conditions are different, the assumptions of the solutions in modified Rayleigh-Riata method are same. By using water pressure, the bending experiment of PV panel was completed. Two boundary conditions were realized by changing the test frame. Comparing the theoretical results with experimental results, the accuracy of the analytical solutions are verified. The influences of boundary condition are also concluded. The theoretical model and solutions obtained in this paper could be the foundations to the optimal work in future, and some suggestions for the installation ways of double glass PV panel can be made based on those works.

2. Theoretical analysis of double glass PV panel with two boundary conditions

A mechanical model is built to describe the bending behaviour of the double glass PV panel under uniformly distributed force, and then, the deflections of whole panel with two different boundary conditions are solved. Hoff model is used in present paper and the corresponding governing equations are developed. Then, the boundary equations are given based on boundary conditions and internal force formulas of laminate plate. Although the boundary equations are different, the assumptions of the solutions in present paper are same as a general assumptions. Rayleigh-Rita method is modified to solve the deflections of whole double glass PV panel. At last, the strain and stress are calculated based on those bending deflections.

2.1. Mechanical model and basic hypothesis

In Fig. 1, it shows the basic components of PV panel, including cover glass, ethylene-vinylacetate (EVA), silicon solar cells and back glass. Silicon solar cells are embedded in the EVA layer to be protected. Based on Naumenko and Eremeyev [18], the bending moment and normal force could be negligible in the EVA layer, but the shear stress should be transmitted by EVA. In order to simplify the problem, a laminate plate model is applied and several hypothesises are made same as [23].

(1) The cover and backboard glasses are treated as top and bottom surfaces of the laminate plate, respectively. And both of them are simulated as isotropic plates with constant flexural rigidity.
(2) The silicon solar cells are too thin to bear any shear stress, and the two EVA layers play the main role of interlayer. The silicon solar cells layer is ignored and two EVA layers are merged as one layer which is defined as the interlayer only made of EVA. The whole PV panel is simplified as a three-layer composite, including cover plate, interlayer and back plate. The mechanical model of PV panel under uniformly distributed force and the corresponding coordinate system are shown in Fig. 2.
(3) According to the research results summarized by Naumenko and Eremeyev [18] and Stefan-H. Schulze etc. [22], in PV module, the ratio of the shear moduli between interlayer and surface layer is in the range between 10^{-5} and 10^{-2}. The PV module is a typical soft core laminate plate and the stress of the interlayer in x-y plan should be ignored.
(4) Only the anti-symmetrical deformation is studied in present paper, so the stress σ_z and the strain ε_z of interlayer are very small and can be ignored, which is defined as $\sigma_z = 0, \varepsilon_z = 0$.

2.2. Hoff model and governing equations

Reissner theory is modified by Hoff [48], and a Hoff model is developed for the laminated plate. In Hoff model, the flexural rigidities of surface plates must be calculated but the interlayer is a relative soft layer. According to Hoff model and those hypothesises in section 2.1, the governing equations of the PV panels can be derived same as [23] as

$$D\left(\frac{\partial^2\varphi_x}{\partial x^2}+\frac{1-\nu_f}{2}\frac{\partial^2\varphi_x}{\partial y^2}+\frac{1+\nu_f}{2}\frac{\partial^2\varphi_y}{\partial x\partial y}\right)+C\left(\frac{\partial w}{\partial x}-\varphi_x\right)=0 \tag{1}$$

$$D\left(\frac{\partial^2\varphi_y}{\partial y^2}+\frac{1-\nu_f}{2}\frac{\partial^2\varphi_y}{\partial x^2}+\frac{1+\nu_f}{2}\frac{\partial^2\varphi_x}{\partial x\partial y}\right)+C\left(\frac{\partial w}{\partial y}-\varphi_y\right)=0 \tag{2}$$

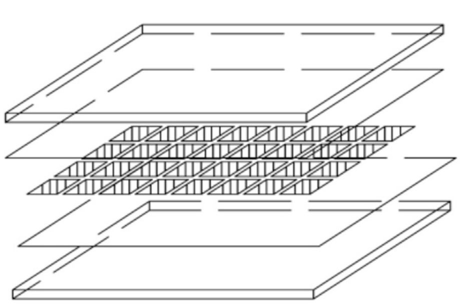

Fig. 1. Structural diagram of monocrystalline silicon double glass photovoltaic panel.

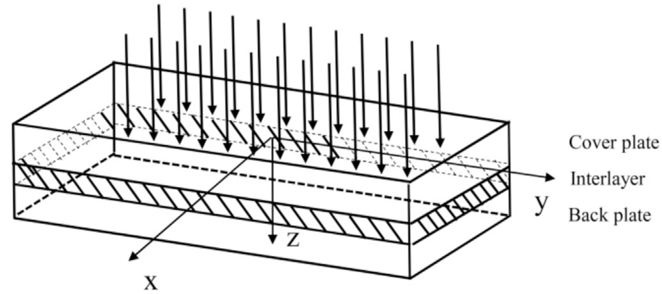

Fig. 2. Mechanical model of PV panel and corresponding coordinate system.

$$C\left(\nabla^2 w-\frac{\partial\varphi_x}{\partial x}-\frac{\partial\varphi_y}{\partial y}\right)-2D_f\nabla^2\nabla^2 w+q=0 \tag{3}$$

where φ_x, φ_y and w are unknown variables as cross section rotation at x-z plane, y-z plane and deflection at z direction, respectively. Constant variables D, D_f and C are calculated as equation (9) to equation (11). In order to simplify the governing equations, two functions ω and f are introduced and they are defined as equation (4) and equation (5).

$$\varphi_x=\frac{\partial\omega}{\partial x}+\frac{\partial f}{\partial y} \tag{4}$$

$$\varphi_y=\frac{\partial\omega}{\partial y}-\frac{\partial f}{\partial x} \tag{5}$$

With equations (1)–(3) and equations (4) and (5), the modified governing equations of PV panel under uniformly distributed force can be written as

$$w=\omega-\frac{D}{C}\nabla^2\omega \tag{6}$$

$$\left(D+2D_f\right)\nabla^2\nabla^2\omega-\frac{2DD_f}{C}\nabla^2\nabla^2\nabla^2\omega=q \tag{7}$$

$$\frac{1}{2}D\left(1-\nu_f\right)\nabla^2 f-Cf=0 \tag{8}$$

with

$$D=\frac{E_f(h+t)^2 t}{2\left(1-\nu_f{}^2\right)} \tag{9}$$

$$D_f=\frac{E_f t^3}{12\left(1-\nu_f{}^2\right)} \tag{10}$$

$$C=G_C\frac{(h+t)^2}{h} \tag{11}$$

where E_f is the elastic modulus of the cover and the back glass plate, ν_f is the Poisson's ratio of the cover and the back glass plate, G_C is the shear modulus of EVA, t and h are the thickness of surface plate and EVA interlayer, respectively.

2.3. Boundary conditions and boundary equations

The installtion ways of PV panel integrated into the building have different options, depending on the position of building. Two boundary conditions which can simulate the usual two installtion ways are studied in present paper. One of them is SSSS and the other one is SSFF. As shown in Fig. 3, the whole PV panel is simply supported at four edges: $x = 0$, a and $y = \pm 0.5b$. In Fig. 4, the PV panel is simply supported at the edges $x = 0$ and a, and free-free at the edges $y = \pm 0.5b$.

If the boundary condition is SSSS, it should satisfy the formulas as follows.

$$(M_x^{'})_{x=0,a} = 0, (w)_{x=0,a} = 0, (\varphi_y)_{x=0,a} = 0, (M_x^{''})_{x=0,a} = 0 \quad (12)$$

$$\left(M_y^{'}\right)_{y=\pm\frac{b}{2}}=0, (w)_{y=\pm\frac{b}{2}}=0, (\varphi_x)_{y=\pm\frac{b}{2}}=0, \left(M_y^{''}\right)_{y=\pm\frac{b}{2}} = 0 \quad (13)$$

If the boundary condition is SSFF, the following formular must be satisfied.

$$(M_x^{'})_{x=0,a} = 0, (w)_{x=0,a} = 0, (\varphi_y)_{x=0,a} = 0, (M_x^{''})_{x=0,a} = 0 \quad (14)$$

$$\left(M_y^{'}\right)_{y=\pm\frac{b}{2}}=0, \left(M_{xy}^{'}\right)_{y=\pm\frac{b}{2}}=0\left(M_{xy}^{''}\right)_{y=\pm\frac{b}{2}}=0, (Q_y)_{y=\pm\frac{b}{2}}=0, \left(M_y^{''}\right)_{y=\pm\frac{b}{2}} = 0 \quad (15)$$

1. Boundary equations of SSSS

At the edges $x = 0$, a and $y = \pm 0.5b$, equation (12) and equation (13) can be derived out as follows.

$$\frac{\partial\varphi_x}{\partial x} = 0, \varphi_y = 0, w = 0, \frac{\partial^2 w}{\partial x^2} = 0 \quad (16)$$

$$\frac{\partial\varphi_y}{\partial y} = 0, \varphi_x = 0, w = 0, \frac{\partial^2 w}{\partial y^2} = 0 \quad (17)$$

Combining with equations (4) and (5) and following the procedure derived by previous research work [23], we can obtain equation (18) and equation (19) based on equation (16) and equation (17).

$$\omega = \nabla^2\omega = \nabla^4\omega = 0, \frac{\partial f}{\partial x} = 0 \quad (18)$$

$$\omega = \nabla^2\omega = \nabla^4\omega = 0, \frac{\partial f}{\partial y} = 0 \quad (19)$$

Equation (18) and equation (19) are just the boundary equations of SSSS, and they will be applied in next section to calculate the deflection of PV panel.

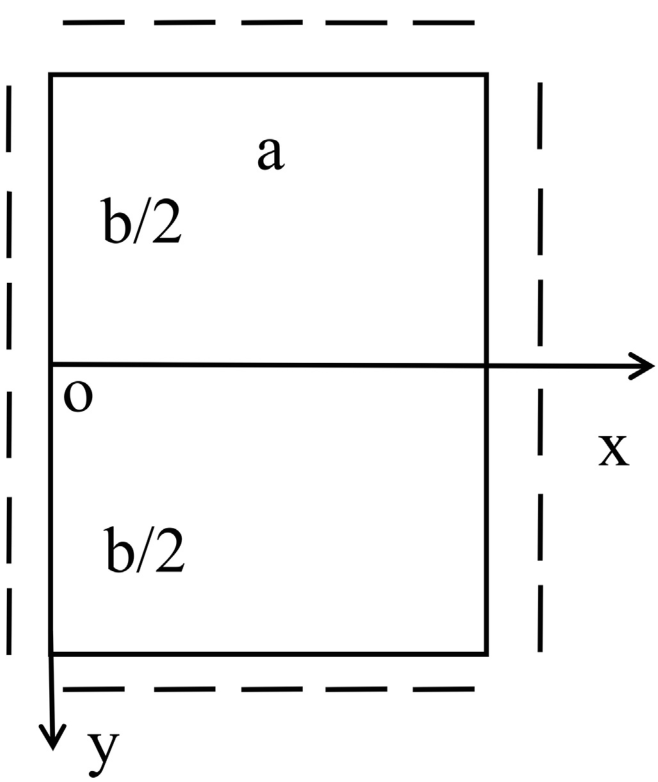

Fig. 3. Boundary condition of PV panel: four edges simply supported.

2. Boundary equations of SSFF

At the edges $x = 0$ and a, equation (14) are the same as equation (12). The boundary equations should be the same as equation (18) for those two simply supported edges.

At the edges $y = \pm 0.5b$, the boundary condition is different. According to the stress-strain relationship of laminated plate [47], equation (15) could be rewritten as follows.

$$-D\left(\frac{\partial\varphi_y}{\partial y} + \nu_f\frac{\partial\varphi_x}{\partial x}\right) = 0 \quad (20)$$

$$-2D_f\left(\frac{\partial^2 w}{\partial y^2} + \nu_f\frac{\partial^2 w}{\partial x^2}\right) = 0 \quad (21)$$

$$-\frac{1}{2}\left(1-\nu_f\right)D_f\left(\frac{\partial\varphi_x}{\partial y} + \frac{\partial\varphi_y}{\partial x}\right) = 0 \quad (22)$$

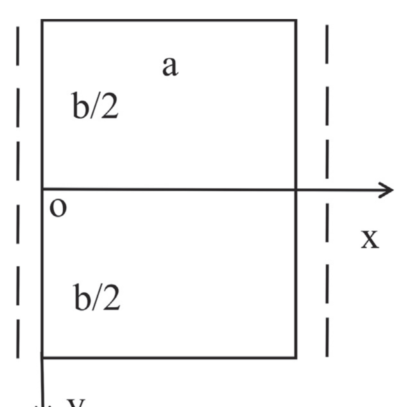

Fig. 4. Boundary condition of PV panel: two edges simply supported, two edges free.

$$-2\left(1-\nu_f\right)D_f\frac{\partial^2 w}{\partial x\partial y}=0 \tag{23}$$

$$C\left(\frac{\partial w}{\partial y}-\varphi_y\right)-2D_f\left(\frac{\partial^3 w}{\partial x^2\partial y}+\frac{\partial^3 w}{\partial y^3}\right)=0 \tag{24}$$

From derivations made by the authors in Ref. [23], the boundary equations of two free edges could be as

$$\frac{\partial^2\omega}{\partial y^2}-\frac{\partial^2 f}{\partial x\partial y}+\nu_f\frac{\partial^2\omega}{\partial x^2}+\nu_f\frac{\partial^2 f}{\partial x\partial y}=0 \tag{25}$$

$$\frac{\partial^2\omega}{\partial y^2}-\frac{D}{C}\left(\frac{\partial^4\omega}{\partial x^2\partial y^2}+\frac{\partial^4\omega}{\partial y^4}\right)+\nu_f\frac{\partial^2\omega}{\partial x^2}--\frac{D}{C}\nu_f\left(\frac{\partial^4\omega}{\partial x^4}+\frac{\partial^4\omega}{\partial x^2\partial y^2}\right)=0 \tag{26}$$

$$\frac{\partial^2\omega}{\partial x\partial y}-\frac{D}{C}\left(\frac{\partial^4\omega}{\partial x^3\partial y}+\frac{\partial^4\omega}{\partial x\partial y^3}\right)=0 \tag{27}$$

$$\begin{aligned}&-D\left(\frac{\partial^3\omega}{\partial x^2\partial y}+\frac{\partial^3\omega}{\partial y^3}\right)+C\frac{\partial f}{\partial x}-2D_f\left[\frac{\partial^3\omega}{\partial x^2\partial y}+\frac{\partial^3\omega}{\partial y^3}-\frac{D}{C}\left(\frac{\partial^5\omega}{\partial x^4\partial y}\right.\right.\\&\quad\left.\left.+2\frac{\partial^5\omega}{\partial x^2\partial y^3}+\frac{\partial^5\omega}{\partial y^5}\right)\right]\\&\quad=0\end{aligned} \tag{28}$$

Equations (18), and (25) − (28) are the specific boundary equations of SSFF. They will be applied in the next derivation work for closed-form solution of deflection.

2.4. Modified Rayleigh-Rita method and closed-form solutions

Rayleigh-Rita method uses the expansion of the unknown deflection functions in infinite series form. It is possible to approach or be close to the exact solutions of the equations by taking the sufficient number of the terms in the series.

2.4.1. Closed-form solutions of SSSS

2.4.1.1. Classical method - Navier method. In previous researches, the specific assumptions of the solutions to the governing equations are different due to different boundary conditions. To the laminate plate with four edges simply supported, the assumption of solution in equation (7) is usually as

$$\omega=\sum_{m=1}^{\infty}\sum_{n=1}^{\infty}A_{mn}\sin\left(\frac{m\pi y}{b}\right)\sin\left(\frac{n\pi x}{a}\right) \tag{29}$$

where A_{mn} is unknown variable needed to be solved.

Substituting equation (29) into the governing equation (7), the partial differential equation is transformed as an algebraic equation.

$$\begin{bmatrix}A_1\left(\frac{n\pi}{a}\right)^4+2A_1\left(\frac{n\pi}{a}\right)^2\left(\frac{m\pi}{b}\right)^2+A_1\left(\frac{m\pi}{b}\right)^4+A_2\left(\frac{n\pi}{a}\right)^6\\+3A_2\left(\frac{n\pi}{a}\right)^4\left(\frac{m\pi}{b}\right)^2+3A_2\left(\frac{n\pi}{a}\right)^2\left(\frac{m\pi}{b}\right)^4+A_2\left(\frac{m\pi}{b}\right)^6\end{bmatrix}\omega=q \tag{30}$$

and $A_1=D+2D_f$, $A_2=2DD_f/C$.

Bending behaviour of PV panel under uniformly distributed force is studied in present paper, so the force q is a constant. Taking the Fourier expansion and doing odd continuation on the right term in equation (30), it can be expressed as follows.

$$\begin{aligned}q&=\frac{4}{ab}\sum_{m=1}^{\infty}\sum_{n=1}^{\infty}\left[\int_0^a\int_0^b q\sin\frac{n\pi x}{a}\sin\frac{m\pi y}{b}dxdy\right]\sin\frac{n\pi x}{a}\sin\frac{m\pi y}{b}\\&=\frac{4}{ab}\sum_{m=1}^{\infty}\sum_{n=1}^{\infty}\left[\frac{qab}{mn\pi^2}(1-\cos n\pi)(1-\cos m\pi)\right]\sin\frac{n\pi x}{a}\sin\frac{m\pi y}{b}\end{aligned} \tag{31}$$

Substituting equation (31) into equation (30) and reorganizing the terms, so A_{mn} can be solved as

$$A_{mn}=\frac{1}{\Phi}\frac{4}{ab}\frac{qab}{mn\pi^2}(1-\cos n\pi)(1-\cos m\pi) \tag{32}$$

where

$$\Phi=\begin{bmatrix}A_1\left(\frac{n\pi}{a}\right)^4+2A_1\left(\frac{n\pi}{a}\right)^2\left(\frac{m\pi}{b}\right)^2+A_1\left(\frac{m\pi}{b}\right)^4+A_2\left(\frac{n\pi}{a}\right)^6\\+3A_2\left(\frac{n\pi}{a}\right)^4\left(\frac{m\pi}{b}\right)^2+3A_2\left(\frac{n\pi}{a}\right)^2\left(\frac{m\pi}{b}\right)^4+A_2\left(\frac{m\pi}{b}\right)^6\end{bmatrix} \tag{33}$$

The procedure stated above is just the Navier method and it can be only used in the plate structure with four edges simply supported. The assumption of solution, equation (29), is also only suitable for the boundary condition as SSSS.

2.4.1.2. Modified Rayleigh-Rita method. In present paper, a modified Rayleigh-Rita method is applied to solve the governing equations and a modified general assumption is developed for the solutions. Since the boundary condition is simply supported at edges $x=0$ and a, the sinusoidal function should be utilized and the unknown variables ω and f are assumed as

$$\omega=\sum_{n=1}^{\infty}\left(e^{\lambda_n y}\omega_n+\omega^*\right)\sin(k_n x) \tag{34}$$

$$f=\sum_{n=1}^{\infty}e^{\eta_n y}f_n\cos(k_n x) \tag{35}$$

where $k_n=n\pi/a$; $\sum_{n=1}^{\infty}(e^{\lambda_n y}\omega_n)\sin(k_n x)$ and $\sum_{n=1}^{\infty}e^{\eta_n y}f_n\cos(k_n x)$ are the general solutions; $\sum_{n=1}^{\infty}(\omega^*)\sin(k_n x)$ is the specific solution; λ_n, ω_n, ω^*, η_n and f_n are unknown variables needed to be solved.

The general solution of equation (7) is studied firstly, so the assumption of general solution, $\omega=\sum_{n=1}^{\infty}(e^{\lambda_n y}\omega_n)\sin(k_n x)$, is substituted into equation (36).

$$\left(D+2D_f\right)\nabla^2\nabla^2\omega-\frac{2DD_f}{C}\nabla^2\nabla^2\nabla^2\omega=0 \tag{36}$$

By merging the same terms, the characteristic equation is written as

$$\begin{aligned}&A_2\lambda_n^6-\left(A_1+3A_2k_n^2\right)\lambda_n^4+\left(2A_1k_n^2+3A_2k_n^4\right)\lambda_n^2-\left(A_1k_n^4+A_2k_n^6\right)\\&\quad=0\end{aligned} \tag{37}$$

with

$$A_1 = D + 2D_f \tag{38}$$

$$A_2 = \frac{2DD_f}{C} \tag{39}$$

Defining $\overline{a} = A_2$, $\overline{b} = -(A_1 + 3A_2k_n^2)$, $\overline{c} = (2A_1k_n^2 + 3A_2k_n^4)$, $\overline{d} = -(A_1k_n^4 + A_2k_n^6)$, equation (37) is also rewritten as equation (40).

$$\overline{a}\lambda_n^6 + \overline{b}\lambda_n^4 + \overline{c}\lambda_n^2 + \overline{d} = 0 \tag{40}$$

Equation (40) is a sextic equation and there are not extract root formulas for it. However, it could be solved as following. By defining a new variable, $S = \lambda^2 + \frac{\overline{b}}{3\overline{a}}$, equation (40) is transformed as

$$S^3 + PS + R = 0 \tag{41}$$

with

$$P = \frac{1}{\overline{a}}\left(\overline{c} - \frac{\overline{b}^2}{3\overline{a}}\right) \tag{42}$$

$$R = \frac{1}{\overline{a}}\left(\overline{d} + \frac{2\overline{b}^3}{27\overline{a}^2} - \frac{\overline{b}\overline{c}}{3\overline{a}}\right) \tag{43}$$

The roots of the cubic equation (41) can be solved by

$$S_1 = \Delta_1 + \Delta_2, S_2 = \overline{\omega}\Delta_1 + \overline{\omega}^2\Delta_2, S_1 = \overline{\omega}^2\Delta_1 + \overline{\omega}\Delta_2 \tag{44}$$

where $\Delta_1 = \sqrt[3]{-\frac{R}{2} + \sqrt{\left(\frac{R}{2}\right)^2 + \left(\frac{P}{2}\right)^3}}$, $\Delta_2 = \sqrt[3]{-\frac{R}{2} - \sqrt{\left(\frac{R}{2}\right)^2 + \left(\frac{P}{2}\right)^3}}$ and $\overline{\omega} = \frac{-1 \pm i\sqrt{3}}{2}$.

According to the definition of S, the roots of equation (37) are finally solved as $\lambda_{n1}, \lambda_{n2} = \pm i\beta_1$, $\lambda_{n3}, \lambda_{n4} = \pm i\beta_2$ and $\lambda_{n5}, \lambda_{n6} = \pm i\beta_3$, in where the variables β could be calculated by

$$\beta_j = \sqrt{\frac{\overline{b}}{3\overline{a}} - S_j}, j = 1, 2, 3 \tag{45}$$

The six roots of the characteristic equation (37) has been solved and the general solution of equation (7) should be written in the format as equation (46).

$$\overline{\omega} = \sum_{n=1}^{\infty}\left[\sum_{r=1}^{6} e^{\lambda_{nr}y}\omega_{nr}\right]\sin(k_n x) \tag{46}$$

Then, the specific solution of equation (7) should be solved to satisfy equation (47).

$$\left(D + 2D_f\right)\nabla^2\nabla^2\overline{\omega}^* - \frac{2DD_f}{C}\nabla^2\nabla^2\nabla^2\overline{\omega}^* = q \tag{47}$$

Taking the Fourier expansion and doing odd continuation on the right term in equation (47), it can be expressed as

$$q = \frac{2}{a}\sum_{n=1}^{\infty}\left[\int_0^a q \sin\frac{n\pi x}{a}dx\right]\sin\frac{n\pi x}{a} = \sum_{n=1}^{\infty}\left\{\frac{2q}{n\pi}[1 - \cos(n\pi)] \times \right\}\sin\frac{n\pi x}{a} \tag{48}$$

Substituting equation (48) into equation (47), the specific solution can be solved as follows.

$$\overline{\omega}^* = \sum_{n=1}^{\infty}\left\{\frac{2q}{n\pi}[1 - \cos(n\pi)]\frac{1}{A_1k_n^4 + A_2k_n^6}\right\}\sin(k_n x) \tag{49}$$

The full solution of equation (7) consists of the general solution and specific solution, and it could be denoted specifically as

$$\omega = \sum_{n=1}^{\infty}\left\{\left[\sum_{r=1}^{6} e^{\lambda_{nr}y}\omega_{nr}\right] + \frac{2q}{n\pi}[1 - \cos(n\pi)]\frac{1}{A_1k_n^4 + A_2k_n^6}\right\}\sin(k_n x) \tag{50}$$

The same procedure could be applied to solve equation (8) with the solution assumption as shown in equation (35), so the solution of equation (8) could be denoted by

$$f = \sum_{n=1}^{\infty}\left(\sum_{r=1}^{2} e^{\eta_{nr}y} f_{nr}\right)\cos(k_n x) \tag{51}$$

where

$$A_3 = \frac{1}{2}D\left(1 - \nu_f\right) \tag{52}$$

$$\eta_{n1} = \sqrt{\frac{C}{A_3} + k_n^2} \tag{53}$$

$$\eta_{n2} = -\sqrt{\frac{C}{A_3} + k_n^2} \tag{54}$$

The full solutions of equation (7) and equation (8) could be calculated by equation (50) and equation (51), respectively. However, there are total eight unknown variables in the solutions, including ω_{nr} (r = 1 to 6) and f_{nr} (r = 1 and 2). The boundary equations are applied in here to obtain the exact values of those unknown variables. If the boundary condition is four edges simply supported, the boundary equation (19) must be satisfied. Substituting equation (50) and equation (51) into equation (19), the eight unknown variables must satisfy the following equations.

$$\sum_{r=1}^{6}\left(e^{\lambda_{nr}y}\right)\omega_{nr} = -\overline{\omega}^* \tag{55}$$

$$\sum_{r=1}^{6}\left(\lambda_{nr}^2 - k_n^2\right)e^{\lambda_{nr}y}\omega_{nr} = \overline{\omega}^* k_n^2 \tag{56}$$

$$\sum_{r=1}^{6}\left(k_n^4 + \lambda_{nr}^4 - 2k_n^2\lambda_{nr}^2\right)e^{\lambda_{nr}y}\omega_{nr} = -k_n^4\overline{\omega}^* \tag{57}$$

$$\sum_{r=1}^{2}(\eta_{nr})e^{\eta_{nr}y}f_{nr} = 0 \tag{58}$$

Substituting y = $\pm 0.5b$, there are eight equations for eight unknown variables based on equations (55)–(58), and all variables could be solved to get exact values. Once ω is solved by equation (50), the deflection of PV panel under uniformly distributed force could be calculated based on equation (6) as

$$
\begin{aligned}
w &= \omega - \frac{D}{C}\nabla^2\omega \\
&= \sum_{n=1}^{\infty}\left\{\sum_{r=1}^{6} e^{\lambda_{nr}y}\omega_{nr} + \frac{2q}{n\pi}[1-\cos(n\pi)]\frac{1}{A_1k_n^4 + A_2k_n^6}\right\}\sin(\mathrm{k}_n x) \\
&-\frac{D}{C}\sum_{n=1}^{\infty}\left\{\sum_{r=1}^{6}\left[\left(-k_n^2\right)e^{\lambda_{nr}y}\omega_{nr} + \lambda_{nr}^2 e^{\lambda_{nr}y}\omega_{nr}\right] + \left(-k_n^2\right)\frac{2q}{n\pi}[1-\cos(n\pi)]\frac{1}{A_1k_n^4 + A_2k_n^6}\right\}\sin(\mathrm{k}_n x)
\end{aligned}
\tag{59}
$$

2.4.2. Closed-form solutions of SSFF

The modified Rayleigh-Rita method is also applied to solve a special boundary condition: SSFF. Since the PV panel is simply supported at edges x = 0 and a, the sinusoidal function is used for x axis. The unknown variables ω and f are also assumed as equation (34) and equation (35), respectively.

The derivation procedure is same as the one stated in the solutions of PV panel with SSSS until equation (54) and the authors' previous work [23]. Due to the different boundary equations, the eight unknown variables must satisfy the following equations based on equations (18), and (25) – (28).

$$
\begin{aligned}
&\sum_{r=1}^{6}\left[\lambda_{nr}^2 e^{\lambda_{nr}y} + \nu_f\left(-k_n^2\right)e^{\lambda_{nr}y}\right]\omega_{nr} + \sum_{r=1}^{2}\left[\nu_f\eta_{nr}(-k_n)e^{\eta_{nr}y}\right. \\
&\quad \left. - \eta_{nr}(-k_n)e^{\eta_{nr}y}\right]f_{nr} \\
&\quad = \nu_f\overline{\omega}^* k_n^2
\end{aligned}
\tag{60}
$$

$$
\sum_{r=1}^{6}\begin{bmatrix}\lambda_{nr}^2 e^{\lambda_{nr}y} - \frac{D}{C}\lambda_{nr}^2\left(-k_n^2\right)e^{\lambda_{nr}y} - \frac{D}{C}\lambda_{nr}^4 e^{\lambda_{nr}y} \\ +\nu_f\left(-k_n^2\right)e^{\lambda_{nr}y} - \nu_f\frac{D}{C}k_n^4 e^{\lambda_{nr}y} - \nu_f\frac{D}{C}\lambda_{nr}^2\left(-k_n^2\right)e^{\lambda_{nr}y}\end{bmatrix}\omega_{nr} = \nu_f\overline{\omega}^* k_n^2 + \nu_f\frac{D}{C}\overline{\omega}^* k_n^4
\tag{61}
$$

$$
\sum_{r=1}^{6}\left[k_n\lambda_{nr}e^{\lambda_{nr}y} + \frac{D}{C}k_n^3\lambda_{nr}e^{\lambda_{nr}y} - \frac{D}{C}k_n\lambda_{nr}^3 e^{\lambda_{nr}y}\right]\omega_{nr} = 0
\tag{62}
$$

$$
\sum_{r=1}^{6}\begin{bmatrix} D\lambda_{nr}k_n^2 e^{\lambda_{nr}y} - D\lambda_{nr}^3 e^{\lambda_{nr}y} + 2D_f\lambda_{nr}k_n^2 e^{\lambda_{nr}y} - 2D_f\lambda_{nr}^3 e^{\lambda_{nr}y} \\ +\frac{2D_fD}{C}\lambda_{nr}k_n^4 e^{\lambda_{nr}y} + \frac{4D_fD}{C}\lambda_{nr}^3\left(-k_n^2\right)e^{\lambda_{nr}y} + \frac{2D_fD}{C}\lambda_{nr}^5 e^{\lambda_{nr}y}\end{bmatrix}\omega_{nr} + \sum_{r=1}^{2}C(-k_n)e^{\eta_{nr}y}f_{nr} = 0
\tag{63}
$$

Once the new eight unknown variables are solved and get their exact values, ω could still be obtained by equation (50). The deflection of PV panel also should be calculated by equation (59).

3. Finite element analysis of double glass PV panel with two boundary conditions

In order to verify the results of Hoff model and modified Rayleigh-Rita method proposed in present paper, FEM software ANSYS is applied to perform a finite element analysis. The double glass PV panels are simplified as five layers composite structure, including cover glass, ethylene-vinylacetate (EVA), silicon solar cells, EVA and back glass. Since it's too thin to make any influence, the battery layer is assumed as a continuous layer. The material of each layer is simulated as isotropic material and the mechanical properties of them are shown in Table 1. Because it could be layered, SHELL181 composite shell element is used for modeling (as shown in Fig. 5).

Comparing with SOLID element, the SHELL element has one more degree of freedom (DOF), rotation. Therefore, the simulation of boundary condition in PV panel should be very careful. If the boundary condition is SSSS, the nodal constraints in X, Y and Z directions are applied on all four edges but the rotation constraint is used on the two short edges (as shown in Fig. 6). If the boundary condition is SSFF, two long edges parallel to the Y axis should be fixed in the Z direction while the other two short edges parallel to the X axis are completely free. Moreover, the node constraints of both X and Y directions are applied at the four corners (as shown in Fig. 7). The finite element analysis model of PV panel under uniformly distributed force is shown as Fig. 8.

4. Experimental analysis of double glass PV panel with two boundary conditions

4.1. Experimental scheme

The bending test of PV panel is performed at room temperature to verify the structural analysis results aforementioned and detect the real mechanical properties. The 6 specimens are all the double glass photovoltaic modules (as shown in Fig. 9) which are provided by Suzhou Tenghui Photovoltaic Technology Co., Ltd (Changshu, P.R. China). The size of the 6 specimens are 1658 × 995 × 7.4 (unit: mm), in which the cover and back glasses are 3.2 mm and the

Table 1
Material parameter values.

Material	Parameter values		
	Modulus of elasticity/MPa	Poisson ratio	Thickness/mm
Reinforced glass	7.2×10^4	0.2	3.2
Crystalline silicon battery	1.44×10^5	0.28	0.2
EVA	3.5×10	0.3	0.8

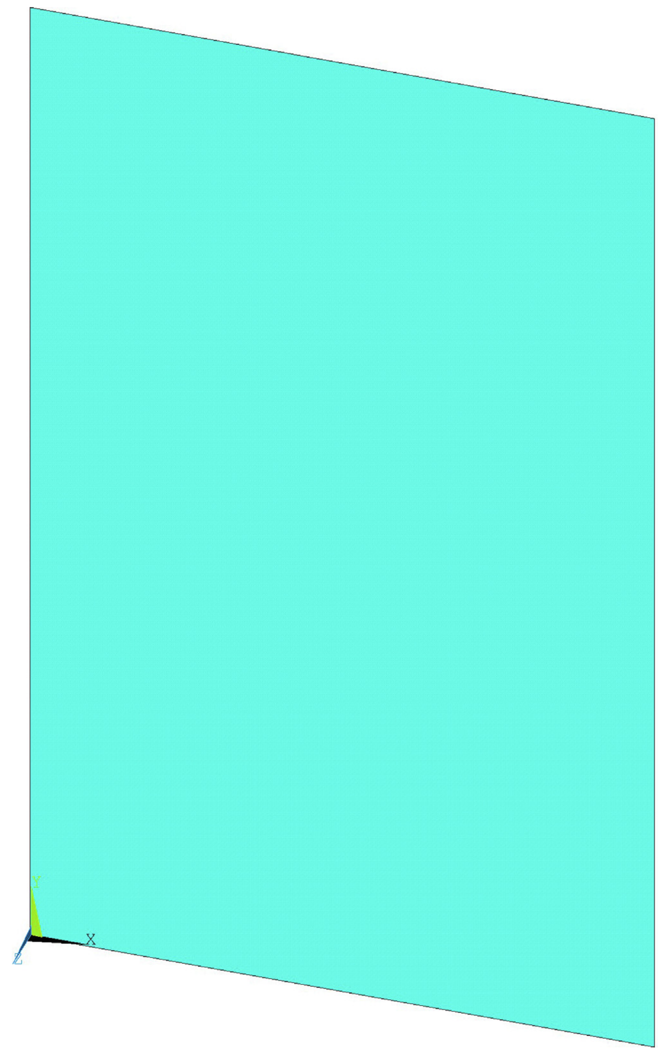

Fig. 5. Finite element analysis model built by SHELL 181 element.

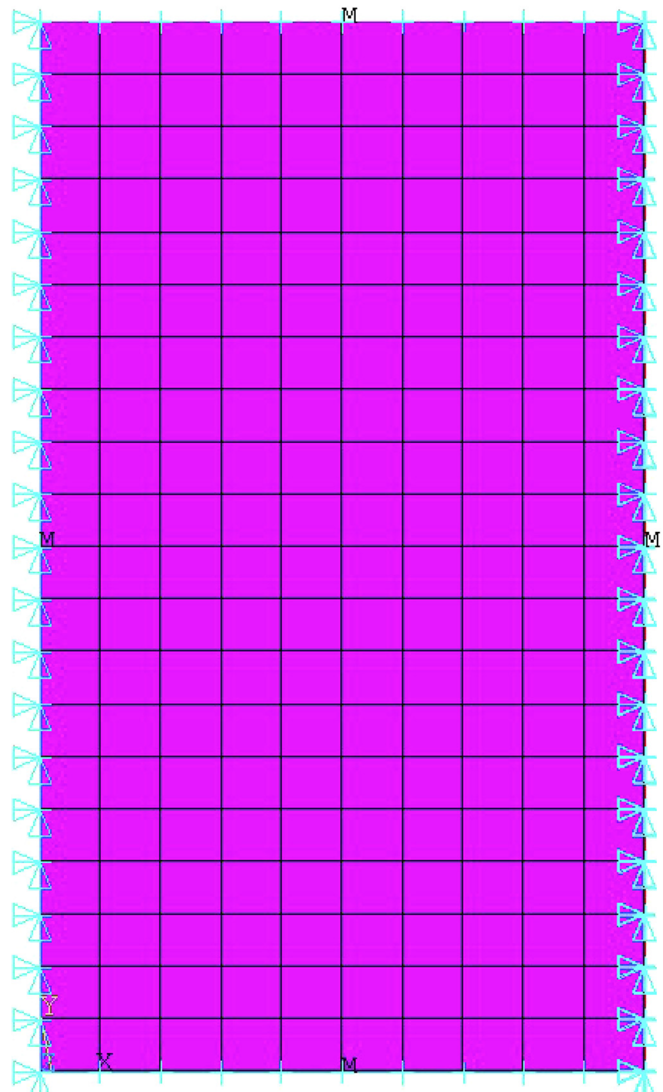

Fig. 6. Boundary condition and mesh of finite element model: SSSS.

interlayer thickness is 1 mm.

The test was completed in National Photovoltaic Product Quality Supervision and Inspection Center at Chengdu. The test procedure is based on current quality inspection certification, IEC 61215 [17]. A test frame (as shown in Fig. 10) is used to mount the PV panel. When it studies SSSS, two steel beams are fabricated and fixed on the two short edges location (as shown in Fig. 11 and Fig. 12). Since the width of the two steel beams and the frame cannot be ignored in that modified frame structure, the actual size of the PV panel under bending should be $1488 \times 855 \times 7.4$ (unit: mm). And the later calculation and simulation should choose that size value. If the boundary condition is SSFF, the frame should be set up as original as shown in Fig. 13 and Fig. 14.

Since it is symmetrical to the shape of PV panel and the loading, the strain measurement points are only set on a quarter part of the panel with total 20 points, which is shown as Fig. 15. DH3816 static strain gauge is used to collect the panel strains, and a laser displacement meter installed under the panel is applied to measure the central deflection. In order to simulate uniformly distributed force better, water pressure is adopted in the tests. There are two loading plans according to the two different boundary conditions. As to the specimens with SSSS, it adds 1 kPa water pressure at each level until 5 kPa, then adds 0.5 kPa to reach their ultimate pressure 5.5 kPa. After that, it unloads 0.5 kPa to 5Kpa and 1Kpa each step until back to 0 kPa (as shown in Fig. 16). When the boundary condition is SSFF, the water pressure is added 1 kPa at each step until

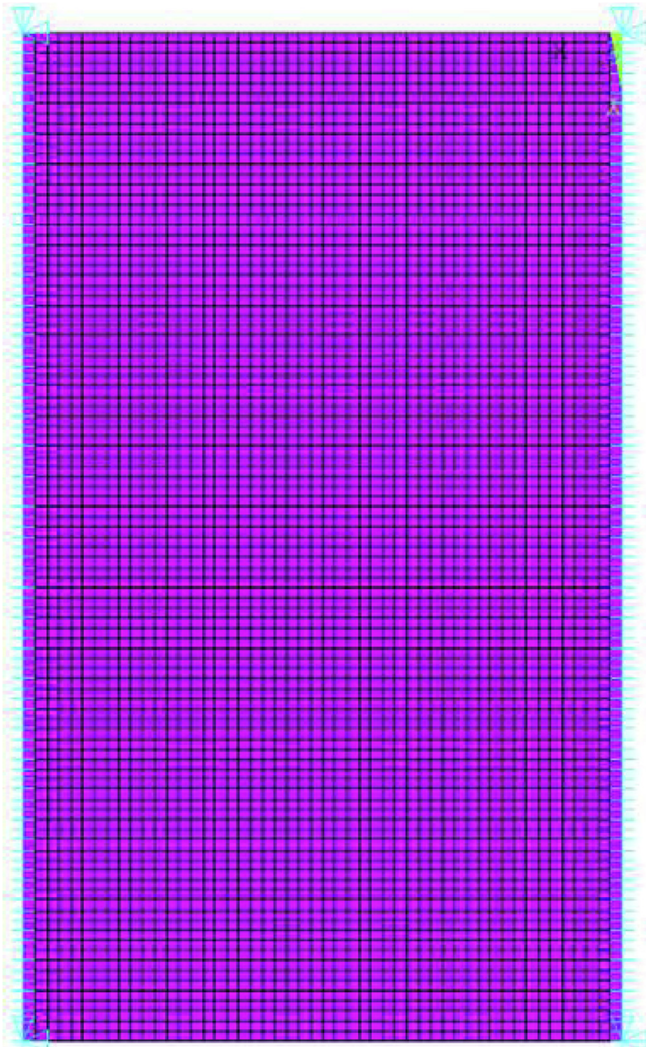

Fig. 7. Boundary condition and mesh of finite element model: SSFF.

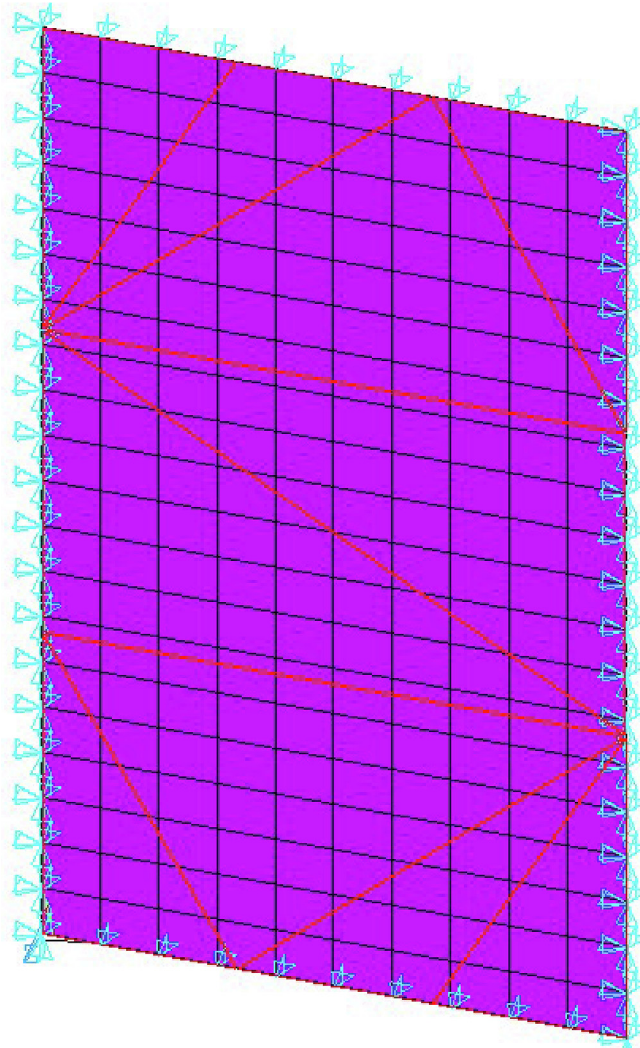

Fig. 8. Finite element model of PV panel under uniformly distributed force.

reaching their ultimate pressure 4 kPa, and it is unloaded 1 kPa for each level until 0 kPa pressure (as shown in Fig. 17). In each stage, the duration time is same as 8min, so the deformation of bending panel can be measured precisely. The test site with frame, PV panel and equipment are just shown as Fig. 18.

4.2. Experiment results

The bending test was completed at 25 °C. The central deflections of the three specimens with SSSS are shown in Table 2 and Fig. 19, and the ones with SSFF are summarized in Table 3 and Fig. 20.

As shown in Table 2 and Fig. 19, the central deflections of PV panels with SSSS are changed nonlinearly with the water pressure. But the deflections measured during the unloading process are almost same as the ones in loading process. When the load is decreased back to 0 kPa, the deflections are very close to 0 mm too and it means there is no residual deflection. All the specimens were checked carefully after the test, and there was not any cracks or breakages on the surface glass. Therefore, the whole deformation of PV panels under 5.5 kPa uniformly distributed force is a safe nonlinear elastic deformation. Moreover, the maximum load is 5.5 kPa and it is more than 2.4 kPa or 5.4 kPa required by current

Fig. 9. Monocrystalline silicon double glass photovoltaic module.

Fig. 10. The test frame for mounting photovoltaic module.

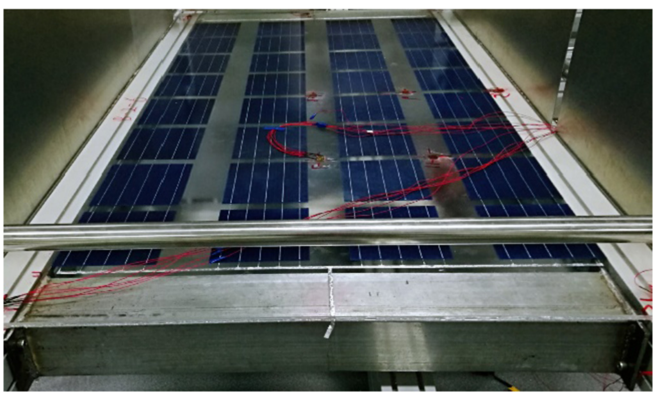

Fig. 11. Four edges simply supported: steel beams at two short edges.

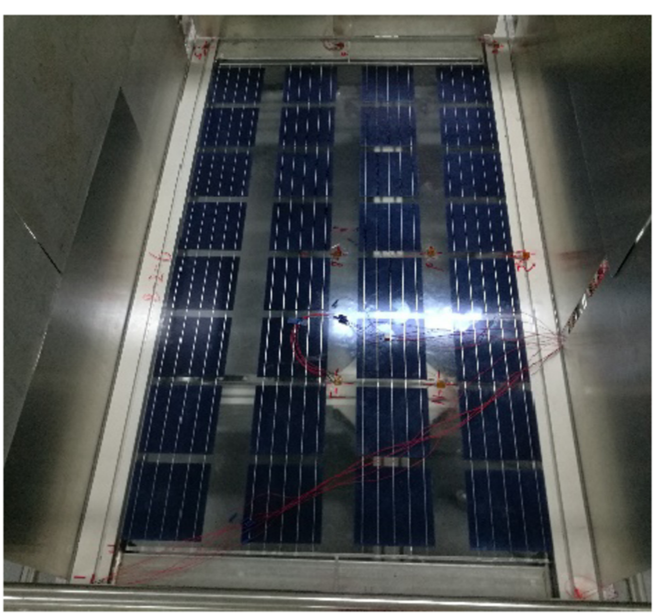

Fig. 12. Four edges simply supported: whole panel is mounted on the frame.

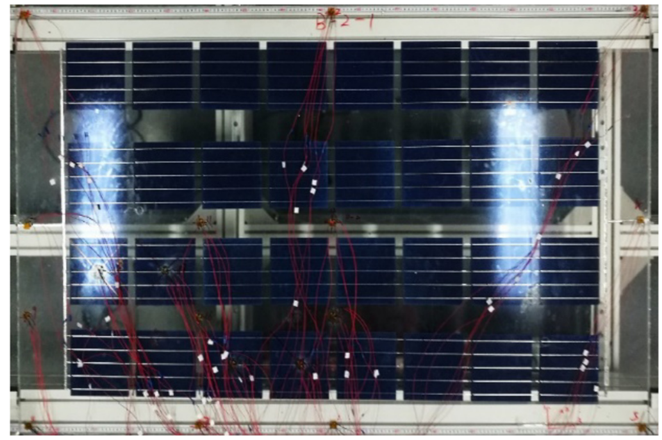

Fig. 13. Two edges simply supported and two edges free: original frame without steel beams at two short edges.

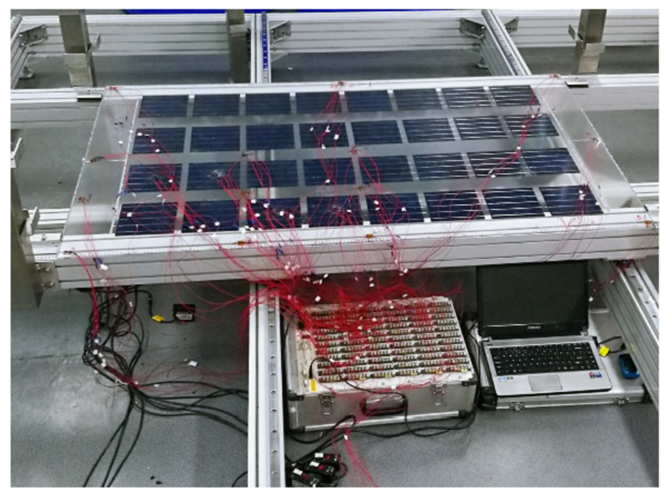

Fig. 14. Two edges simply supported and two edges free: whole panel is mounted on the frame.

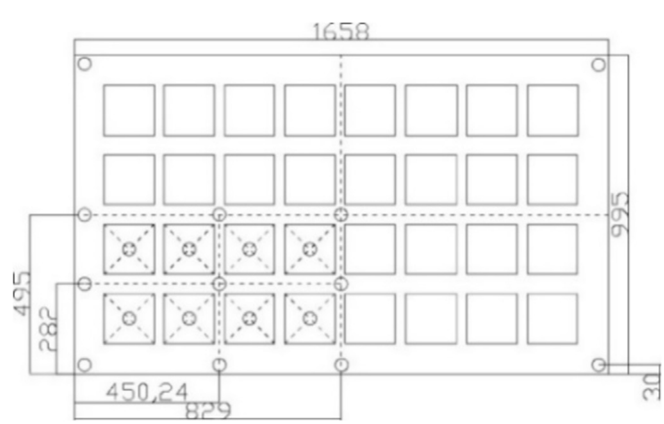

Fig. 15. Arrangement diagram of strain measurement point (unit: mm).

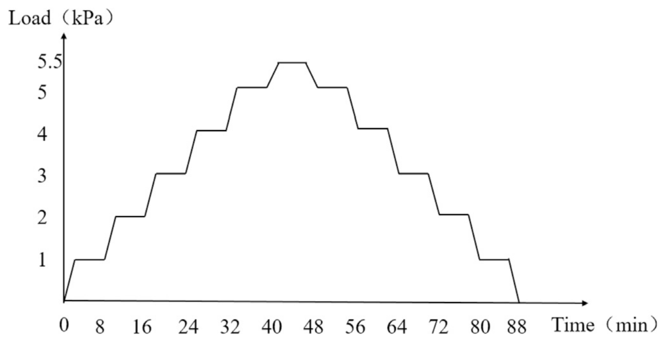

Fig. 16. Test loading scheme for PV panels with SSSS.

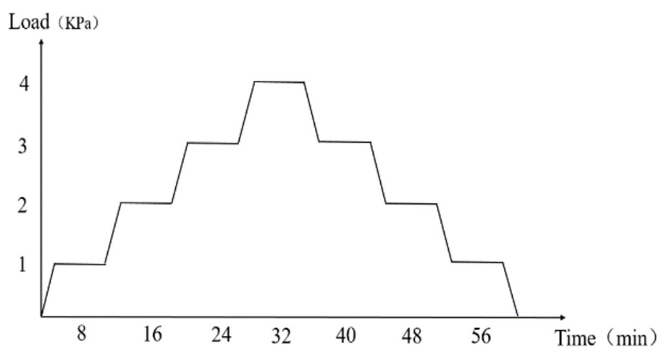

Fig. 17. Test loading scheme for PV panels with SSFF.

Fig. 18. Test site.

certification. It proves that those specimens satisfy the requirements from the certification, IEC 61215 [17]. It's a little different to the PV panels with SSFF, since the central deflections are changed almost linearly with the water pressure and so the whole deformation of those PV panels under 4 kPa is a linear elastic deformation (as shown in Table 3 and Fig. 20). However, the residual deflections of those panels are obvious. It is the first group

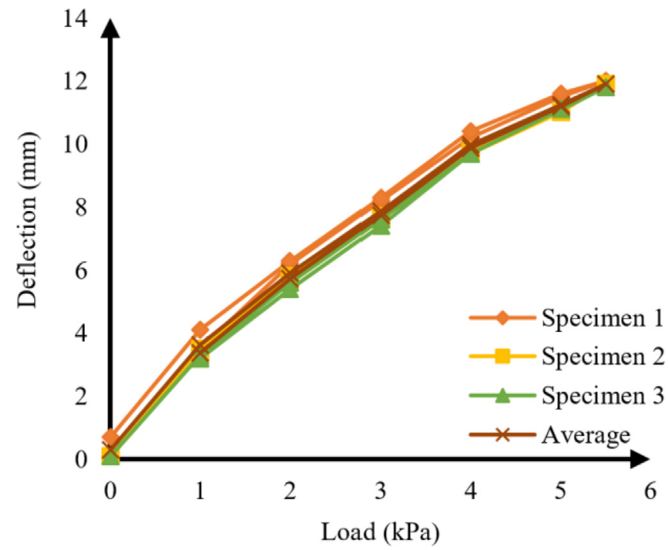

Fig. 19. Test central deflection of PV panels with SSSS.

Table 3
Central deflection of PV panels with SSFF (unit: mm).

Water pressure (kPa)	0	1	2	3	4	3	2	1	0
Specimen 1	0	6.4	10.8	14.4	18.4	14.8	11.2	7.7	3.7
Specimen 2	0	4.4	7.9	12.4	15.7	12	8.8	4.2	1.0
Specimen 3	0	5.9	10.3	14.1	16.9	14	10.6	6.3	1.3

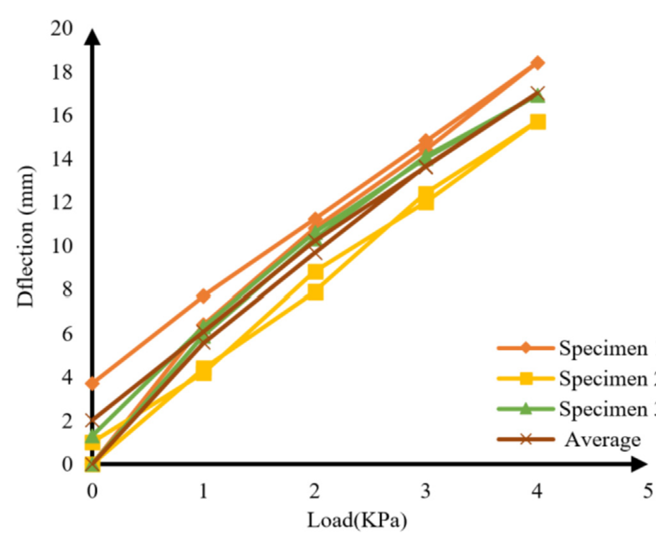

Fig. 20. Text central deflection of PV panels with SSFF.

Table 2
Central deflection of PV panels with SSSS (unit: mm).

Water pressure (kPa)	0	1	2	3	4	5	5.5	5	4	3	2	1	0
Specimen 1	0	3.5	6.2	8.2	10.2	11.5	12	11.6	10.4	8.3	6.3	4.1	0.7
Specimen 2	0	3.4	5.6	7.6	9.7	11	11.9	11	9.8	7.7	5.8	3.5	0.1
Specimen 3	0	3.2	5.4	7.4	9.7	11.1	11.8	11.1	9.7	7.6	5.6	3.3	0.1

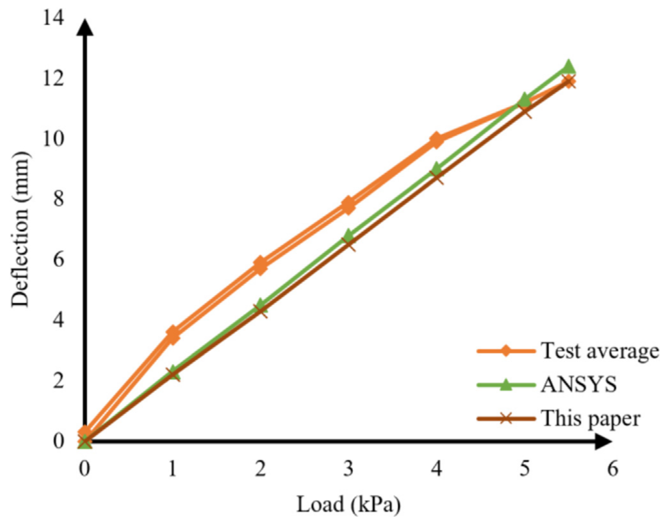

Fig. 21. Central deflection of PV panels with SSSS.

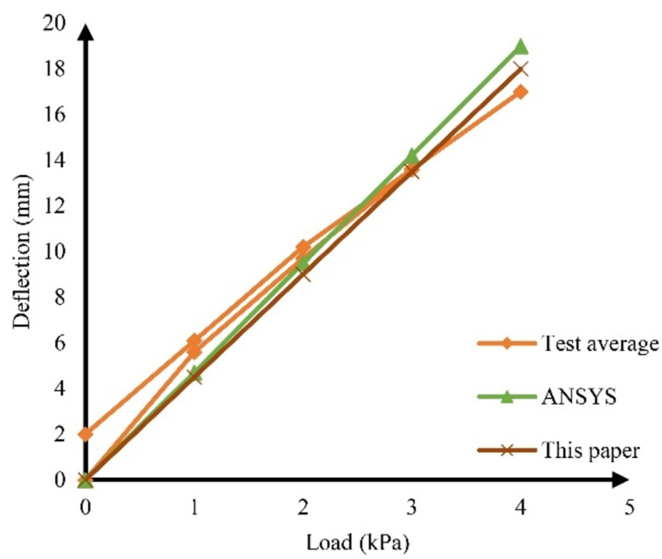

Fig. 22. Central deflection of PV panels with SSFF.

that we tried to do the bending test, and we removed the water by hands in that time. When measuring the central deflections, some water were still on the water proof cloth and it brought the residual deflections. Later, we started to use pumper to remove water from the tank and the residual deflection is much smaller in other group tests.

5. Verifications and discussions

5.1. PV panel deflection

Fig. 21 and Fig. 22 present the central deflections measured by tests, calculated by ANSYS and by equations in present paper. In Table 4 and Table 5, they state the specific values of those deflections.

From Fig. 21 and Table 4, the deflections calculated by both ANSYS and equation (59) are changed linearly with water pressure while the test results are changed nonlinearly. The errors are also very obvious between the test and simulation results. It is because the Hoff model theory is based on linear elastic deformation hypothesis, but the real deformation of PV panels with SSSS under the ultimate pressure is a nonlinear elastic deformation. Although the simulation results are not so good for that boundary condition, there are two things we can learn from them. Firstly, in order to describe that deformation better, a nonlinear elastic theory is supposed to be applied in future study. Secondly, since the simulation results are smaller than test data, it is actually safer to use the simulation to do the design work since the real capability of PV panel will be better. In Table 4, the errors between experimental data and calculation data is much smaller when water pressure is bigger, so the proposed equations are suitable to do the limit state bearing analysis of the PV panel. Moreover, the data from equation (59) are very close to the ones from ANSYS, but the calculation of proposed equation is much faster. So it's suitable to be applied in future optimal design and research.

Fig. 22 and Table 5 state clearly the linear elastic deformation of PV panel with SSFF in the range of 4 kPa water pressure. The results from equation (59) are closer to test results than ANSYS, and the error is only 5.9% when the water pressure approaches the maximum value 4 kPa. The accuracy of the proposed equations in present paper is verified by this group test and simulation. However, the error is still obvious when water pressure is small as 1 kPa. The test operation errors introduced in section 4.2 should be the

Table 4
Central deflection of PV panels with SSSS (unit: mm).

Water pressure (kPa)		0	1	2	3	4	5	5.5	5	4	3	2	1	0
Test average value	Results	0	3.4	5.7	7.7	9.9	11.2	11.9	11.2	10	7.9	5.9	3.6	0.3
ANSYS	Results	0	2.3	4.5	6.8	9	11.3	12.4	11.3	9	6.8	4.5	2.3	0
	Error (%)	0	32.4	21.1	11.7	9.1	0.9	4.2	0.9	10.0	13.9	23.7	36.1	–
This paper	Results	0	2.2	4.3	6.5	8.7	10.9	11.9	10.9	8.7	6.5	4.3	2.2	0
	Error (%)	0	35.3	24.6	15.6	12.1	2.7	0	2.7	13	17.7	27.1	38.9	–

Table 5
Central deflection of PV panels with SSFF (unit: mm).

Water pressure (kPa)		0	1	2	3	4	3	2	1	0
Test average value	Results	0	5.6	9.7	13.6	17.0	13.6	10.2	6.1	2
ANSYS	Results	0	4.7	9.5	14.2	19	14.2	9.5	4.7	0
	Error (%)	0	16.1	2.1	4.4	11.8	4.4	6.9	23	–
This paper	Results	0	4.5	9	13.5	18	13.5	9	4.5	0
	Error (%)	0	19.6	7.2	0.7	5.9	0.7	11.8	26.2	–

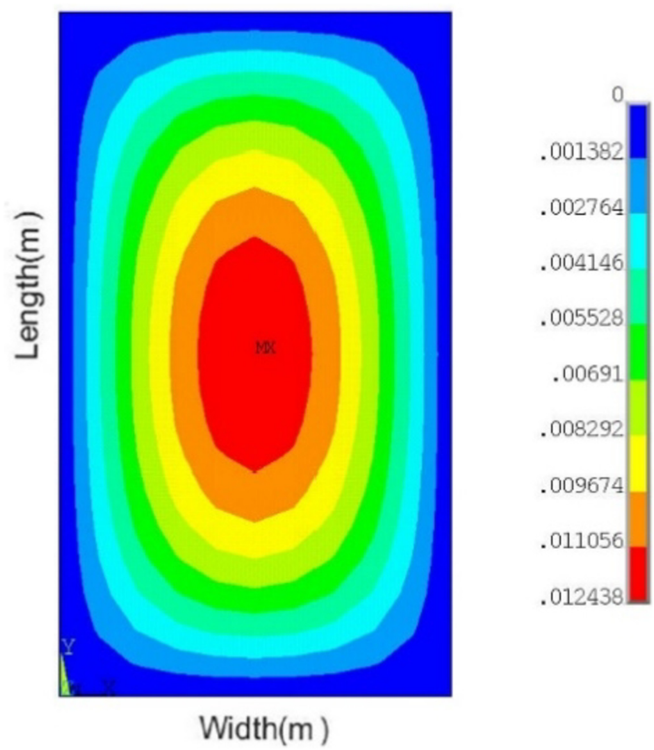

Fig. 23. Deflection nephogram of PV panels with SSSS under 5.5 kPa load, calculated by ANSYS (unit: m).

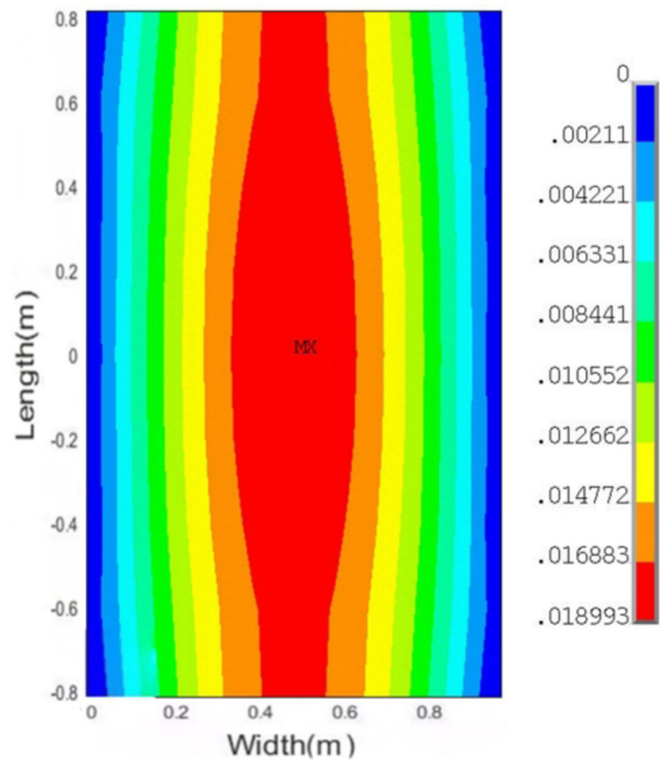

Fig. 25. Deflection nephogram of PV panels with SSFF under 4 kPa load, calculated by ANSYS (unit: m).

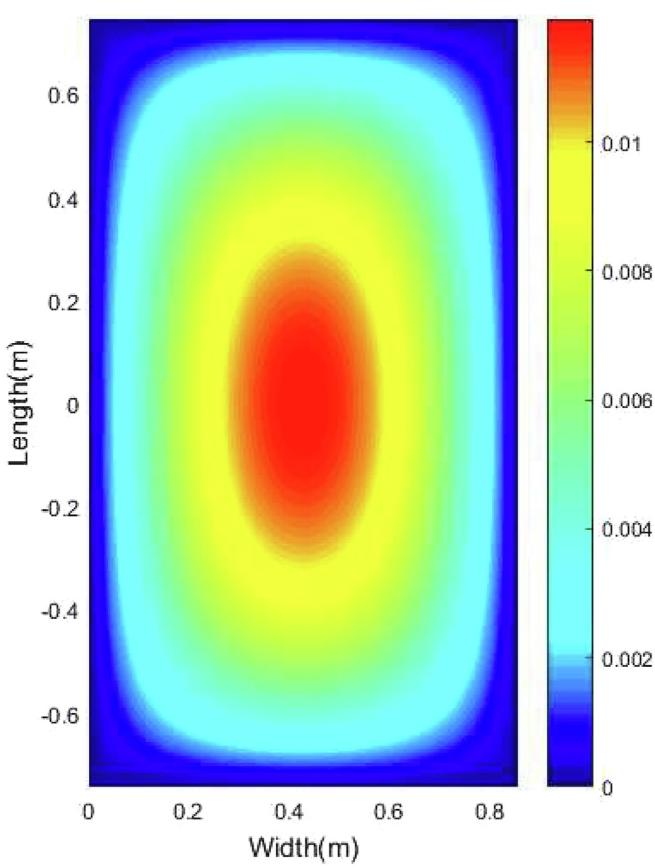

Fig. 24. Deflection nephogram of PV panels with SSSS under 5.5 kPa load, calculated by equations in present paper (unit: m).

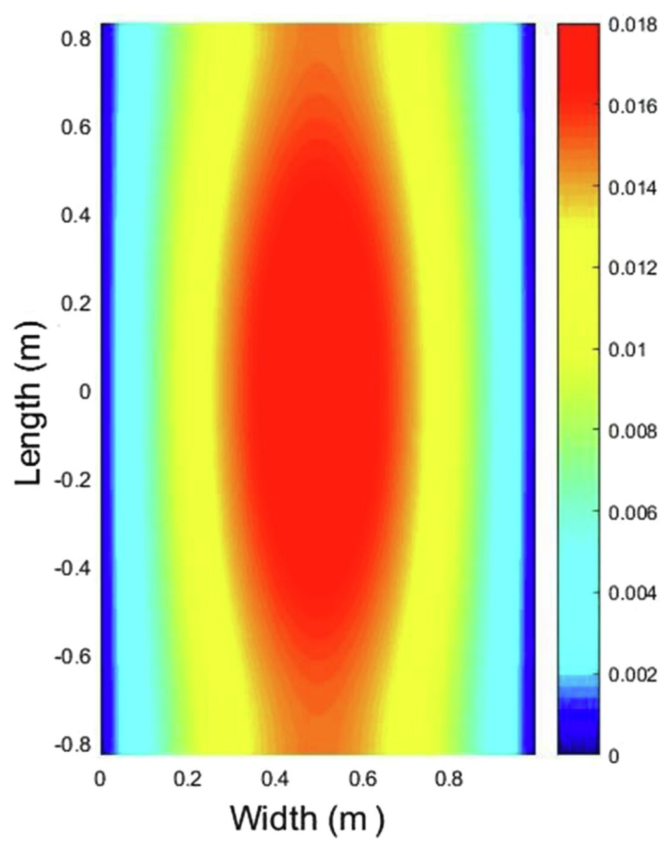

Fig. 26. Deflection nephogram of PV panels with SSFF under 4 kPa load, calculated by equations in present paper (unit: m).

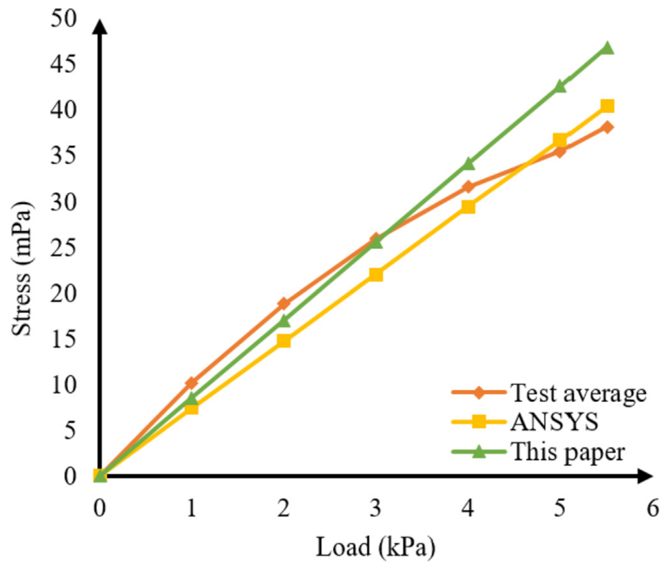

Fig. 27. Central 1st principal stress of PV panels with SSSS.

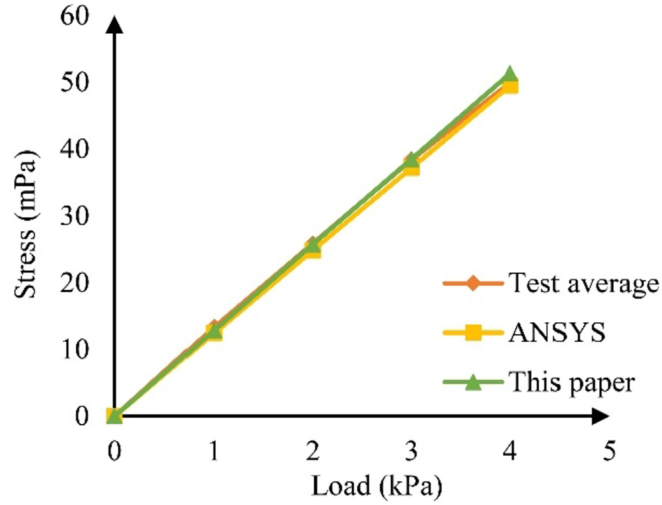

Fig. 28. Central 1st principal stress of PV panels with SSFF.

main reason for those inaccurate results.

Figs. 23–26 show the deflection nephogram of PV panels under the corresponding maximum water pressure. Figs. 23 and 25 are simulated by ANSYS, and Fig. 24 and Fig. 26 are obtained by a MATLAB program based on equation (59). Comparing Fig. 23 with Fig. 24 or Fig. 25 with Fig. 26, the deflection nephogram calculated by proposed equations are very like the ones analysed by ANSYS. Although the proposed equations and ANSYS are not so good to the PV panels with SSSS, the calculation accuracy of them is still all right when water pressure approaches maximum value. In each deflection nephogram, the maximum deflection exists in the middle of the plate and it is 0 on the edges which are simply supported. That shape of plate deflection agrees well with the boundary condition. Moreover, it denotes that the maximum deflections of PV panel with two boundary conditions are both produced at the middle position of the plate, so it should be considered very carefully in future BIPV design work.

5.2. PV panel stress

As shown in Fig. 27 and Table 6, the central 1st principal stress of test is changed nonlinearly with the water pressure while the ones calculated by ANSYS and proposed paper are changed linearly. It is same as the central deflection discussed in section 5.1 and it is indeed nonlinear elastic deformation for the PV panels with SSSS. As to the calculation accuracy, the data from proposed equations are better when the water pressure is small and no more than 3 kPa, but the ones from ANSYS are better under the large water pressure. However, both of them have obvious errors comparing with the test data. In order to describe the nonlinear deformation better and improve the calculation accuracy, a nonlinear elastic theory is supposed to be applied in further study.

Table 7
Central 1st principal stress values of PV panels with SSFF (unit: mPa).

Water pressure (kPa)		0	1	2	3	4
Test average value	Results	0	13.3	25.8	38.4	49.9
ANSYS	Results	0	12.4	24.8	37.2	49.5
	Error (%)	0	6.8	3.9	3.1	0.8
This paper	Results	0	12.8	25.7	38.5	51.3
	Error (%)	0	3.8	0.4	0.3	2.8

As to the PV panels with SSFF, the test stress data has a linear relationship to the water pressure just as the data from ANSYS and proposed equations (as shown in Fig. 28 and Table 7). It proves that the deformation of those PV panels is indeed a linear elastic deformation which is also concluded by the deflection data in section 5.1. Although both proposed equation data and ANSYS date match the experimental data very well, the errors are smaller in proposed equation than ANSYS. The accuracy of the proposed equations on the stress calculation is verified by those comparisons.

Moreover, as shown in both Figs. 27 and 28, the maximum 1st principal stresses on the surface glass of PV panels are all smaller than the limit stress of reinforced glass, so it is safe for the PV panels when they are utilized under those loads.

The 1st principal stress nephogram of PV panels under their own maximum water pressure are shown in Figs. 29 – 32. Figs. 29 and 31 are also simulated by ANSYS, and Fig. 30 and Fig. 32 are obtained by a MATLAB program based on equation (59) and the internal force formulas of laminate plate. Comparing Fig. 29 with Fig. 30 or Fig. 31 with Fig. 32, the stress nephogram calculated by proposed equation are also like the ones analysed by ANSYS, especially to the ones with SSSS. The calculation accuracy of proposed equations on stress is verified by those comparisons. In each 1st principal stress nephogram, the maximum stress exists in the

Table 6
Central 1st principal stress values of PV panels with SSSS (unit: mPa).

Water pressure (kPa)		0	1	2	3	4	5	5.5
Test average value	Results	0	10.2	18.8	25.9	31.6	35.5	38.1
ANSYS	Results	0	7.7	15.3	23	30.7	38.3	42.2
	Error (%)	0	24.2	18.5	11.2	2.8	8.0	10.7
This paper	Results	0	8.5	17	25.5	34.1	42.6	46.8
	Error (%)	0	16.3	9.5	1.5	8.0	20.2	22.8

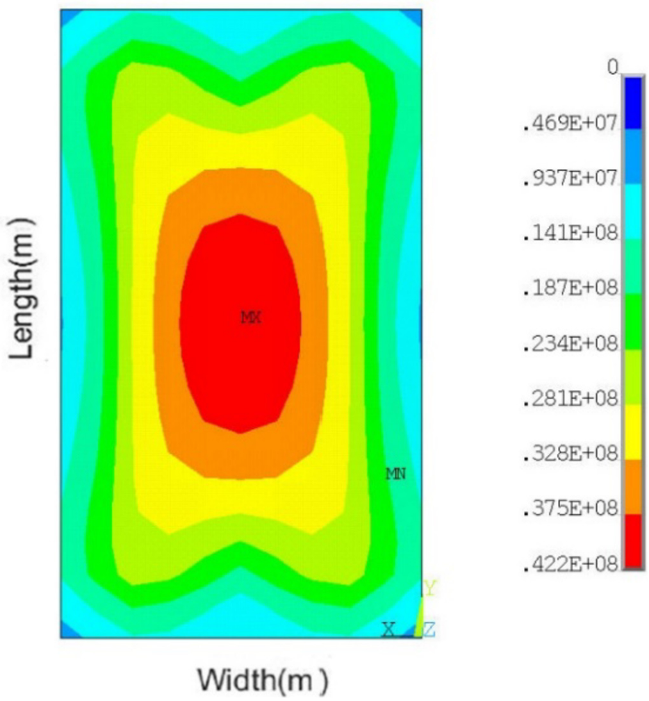

Fig. 29. 1st principal stress nephogram of PV panels with SSSS under 5.5 kPa load, calculated by ANSYS (unit: Pa).

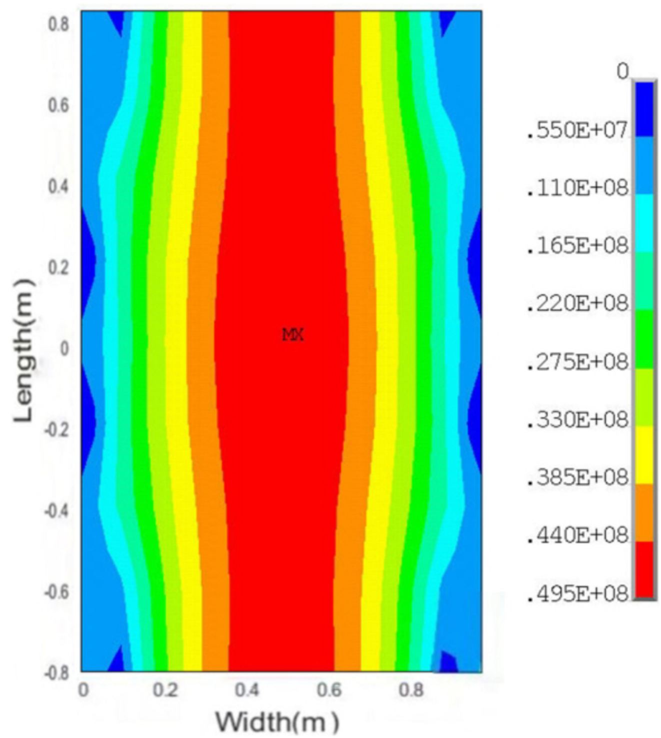

Fig. 31. 1st principal stress nephogram of PV panels with SSFF under 4 kPa load, calculated by ANSYS (unit: Pa).

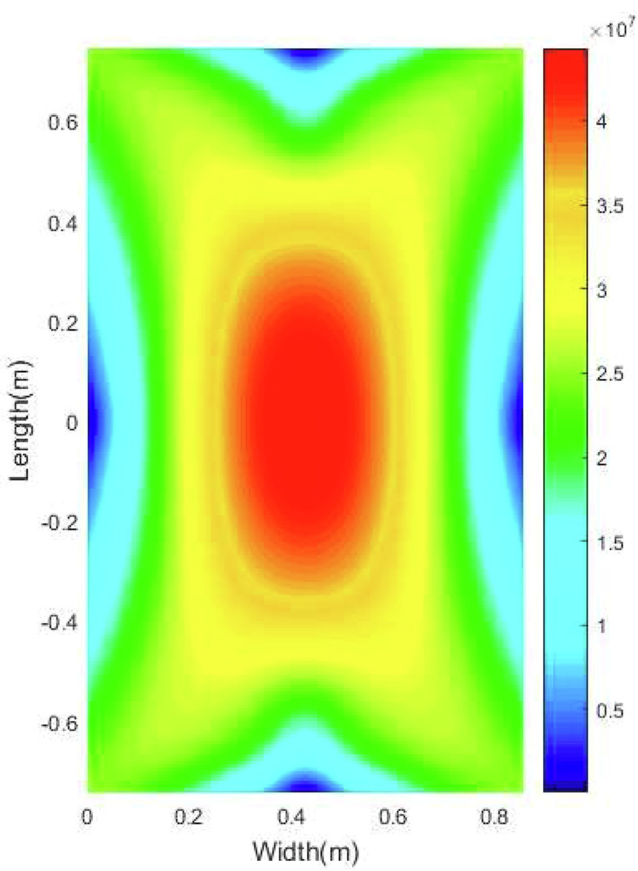

Fig. 30. 1st principal stress nephogram of PV panels with SSSS under 5.5 kPa load, calculated by equations in present paper (unit: Pa).

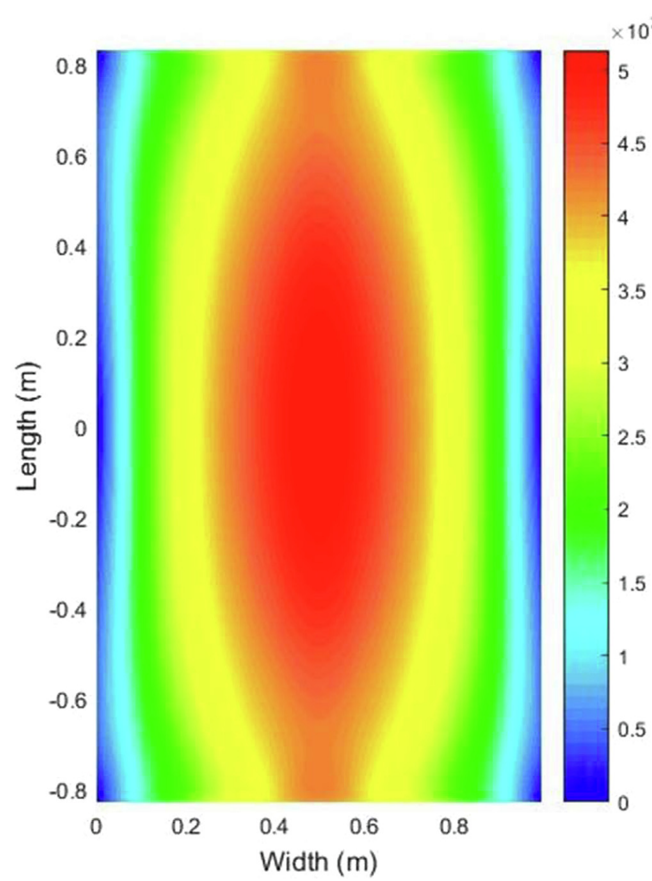

Fig. 32. 1st principal stress nephogram of PV panels with SSFF under 4 kPa load, calculated by equations in present paper (unit: Pa).

middle of the plate and it is 0 on the edges which are simply supported. That shape of plate stress also agrees well with the boundary condition. Moreover, the maximum stress of PV panel with two boundary conditions are both produced at the middle position of the plate. The middle position is a key position to decide the damage of the whole PV panel. In further study on the safety of PV panel, the stress in the middle position should be chosen as the control stress and cannot exceed the limit stress of reinforced glass.

5.3. Influence of boundary condition

Since two different boundary conditions are studied in present paper, some discussions about the influence of boundary condition should be made. The central deflection and central 1st principal stress of PV panels with the two boundary conditions are summarized in Fig. 33 and Fig. 34, respectively. The data from test and proposed equations are stated together.

In Fig. 33, the deflections of PV panels with two different boundary conditions are stated clearly and the ones with SSSS are much better. The ultimate load to the SSSS case is about 5.5 kPa, but it is only 4 kPa to the PV panel with SSFF. Meanwhile, the maximum deflection of SSSS case is around 11.9 mm, and it is much less than 17.0 mm produced by SSFF case. It means the SSSS boundary condition can bear a larger uniformly distributed force with a smaller deflection. The central 1st principal stresses are shown in Fig. 34 and the maximum central stresses of two cases are both close to 50 mPa, which is the limit strength of the reinforced glass. It denotes that the final damage of the whole PV panel is due to the central stress of panel exceeds the limit stress of surface glass. Under the limit stress of surface glass, SSSS case has a larger ultimate load so its mechanical behaviour is proved better than SSFF case again.

The central deflection and central 1st principal stress of PV panels and pure glass panels are summarized in Fig. 35 and Fig. 36, respectively. The data of PV panels are average values from experiments, and the data of pure glass panels are calculated by ANSYS. If the connection between two face glasses is removed, the two pure glasses with 3.2 mm thickness are just put together to bear the force and the data are marked as 3.2 mm glass panel. On contrary, if the connection is strong as the glass material itself, it will be a homogenous glass panel with 7.4 mm thickness and the data are stated as 7.4 mm glass panel. Both SSSS and SSFF are studied to find more conclusions.

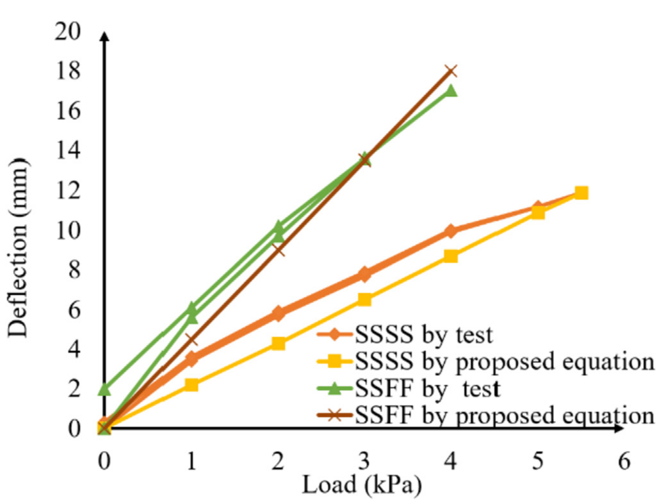

Fig. 33. Central deflection of PV panels with two boundary conditions.

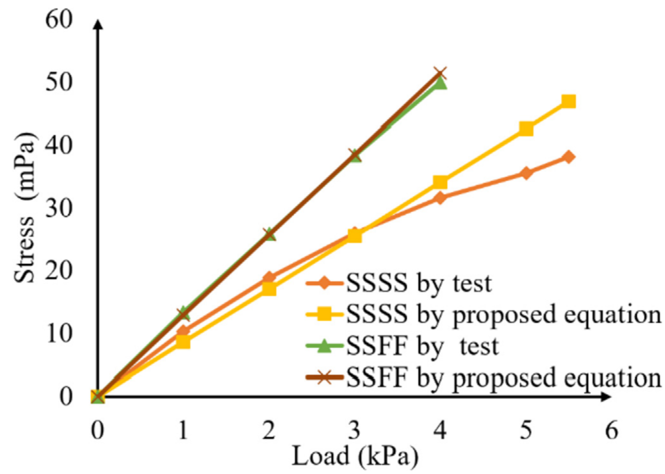

Fig. 34. Central 1st principal stress of PV panels with two boundary conditions.

In both central deflection and central 1st principal stress under the same boundary condition, the data from PV panels are all in a range built by the data from 3.2 mm to 7.4 mm homogenous glass panels (as shown in Figs. 35 and 36). It proves that the mechanical behaviour of double glass PV panel is stronger than two glasses without any connection, but is weaker than one homogenous glass panel with same thickness. It is because the connection effects of interlayer is not strong as glass itself but better than nothing, and that is verified by many theoretical and experimental works before. Considering the 3.2 mm glass panel, the deflection of SSSS under 5.5 kPa load is 62.1 mm, which is much smaller than 93.7 mm deformed in SSFF under 4 kPa. It is same to the 7.4 mm glass panel since SSSS has 10 mm deflection and SSFF has 15.4 mm. The similar conclusion could be made in central 1st principal stress too (as shown in Fig. 36). It is 93.7 mPa under 5.5 kPa in SSSS comparing with 107 mPa under 4 kPa in SSFF if it is 3.2 mm glass panel. In 7.4 mm glass panel, it is 35 mPa versus 40 mPa. Therefore, when the panels are same, the one with SSSS always bears larger load along with smaller deflection and stress, in either PV panels or homogenous glass panels.

Based on the conclusions aforementioned, SSSS boundary condition is a better choice to engineers to design the glass structure and BIPV works, but SSFF boundary condition should be designed very carefully in future.

5.4. Discussions on the proposed method and Navier method

The bending deformation of plate structure with SSSS has been studied for a long time and there is a lot of methods. Among them, Navier method is a very classical method and it has been used in many papers before. In present paper, a modified Rayleigh-Rita method and a general assumption of solution are proposed to study the mechanical properties of PV panel. It is necessary to make some discussions on the results based on different methods. The central deflection and central stress of PV panels with SSSS are presented in Fig. 37 and Fig. 38. The corresponding data values are demonstrated in Table 8 and Table 9. The data from two different methods and the test are stated together.

As shown in Figs. 37 and 38, the data from both proposed method and Navier method are a linear deformation while the test data is a nonlinear deformation. The values of central deflection and central stress from Navier method are all smaller than the values from proposed method. So it is more conservative to choose Navier method to do the design work in BIPV. In

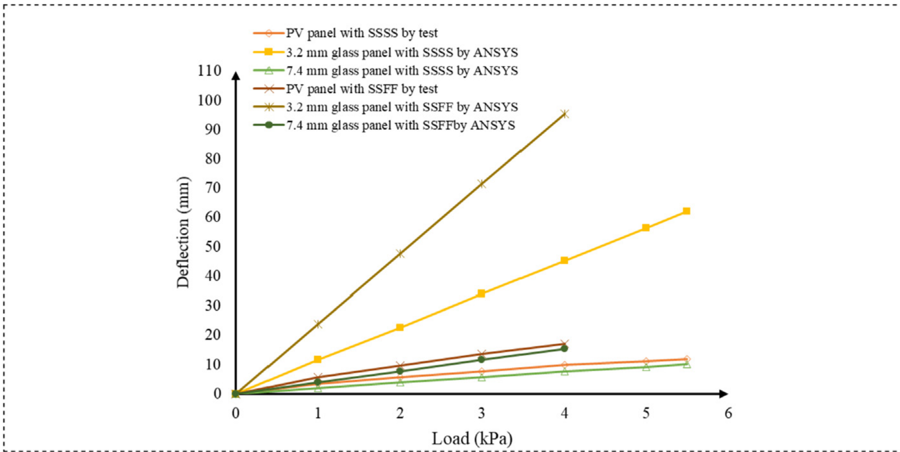

Fig. 35. Central deflection of PV panels and glass panels with two boundary conditions.

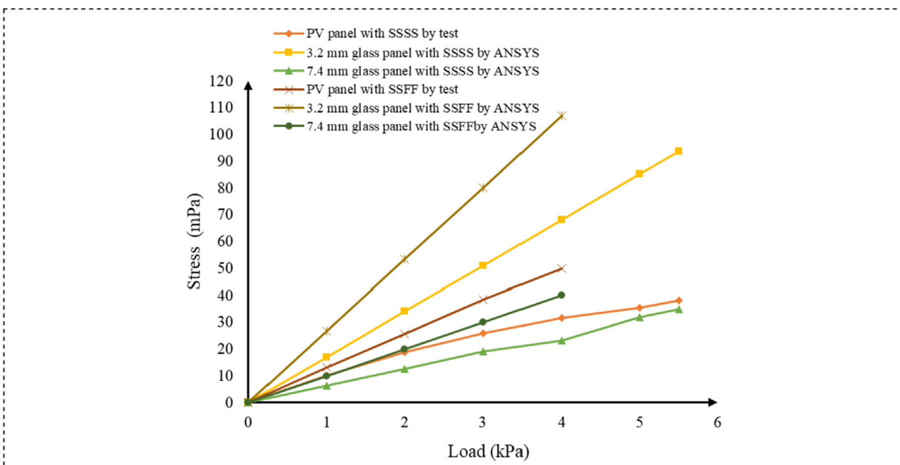

Fig. 36. Central 1st principal stress of PV panels and glass panels with two boundary conditions.

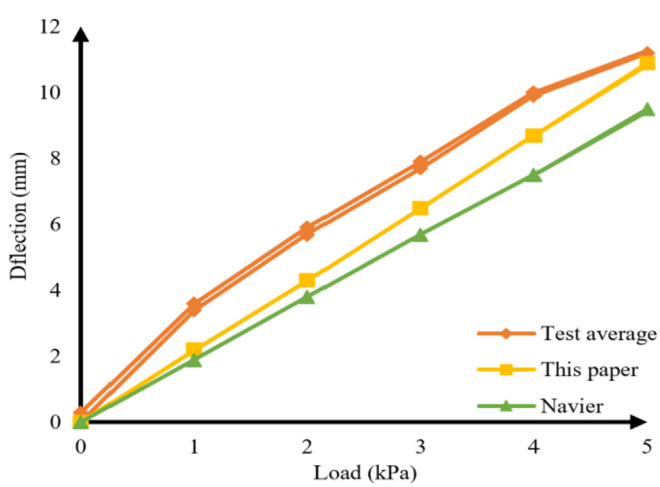

Fig. 37. Central deflection of PV panels with SSSS.

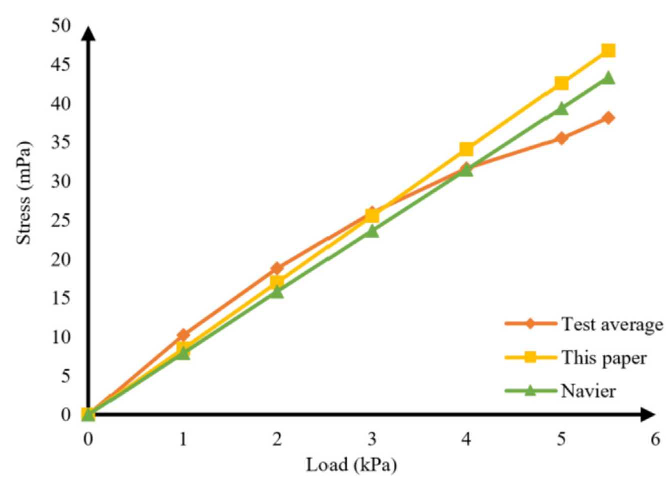

Fig. 38. Central 1st principal stress of PV panels with SSSS.

Fig. 37 and Table 8, the errors of equation (59) are all smaller than Navier method and the maximum central deflection is calculated very accurately by proposed method. It's a little different for the central 1st principal stress in Fig. 38 and Table 9. When water pressure is small, the proposed method is better but Navier method is better to calculate central stress when water pressure is large. Therefore, the proposed method in present paper is better than Navier method to describe the small

Table 8
Central deflection of PV panels with SSSS (unit: mm).

Water pressure (kPa)		0	1	2	3	4	5	5.5	5	4	3	2	1	0
Test average value	Results	0	3.4	5.7	7.7	9.9	11.2	11.9	11.2	10	7.9	5.9	3.6	0.3
This paper	Results	0	2.2	4.3	6.5	8.7	10.9	11.9	10.9	8.7	6.5	4.3	2.2	0
	Error (%)	0	35.3	24.6	15.6	12.1	2.7	0	2.7	13	17.7	27.1	38.9	–
Navier method	Results	0	1.9	3.8	5.7	7.5	9.5	10.4	9.5	7.5	5.7	3.8	1.9	0
	Error (%)	0	44.1	33.3	26.0	24.2	15.2	12.6	15.2	25.0	27.8	35.6	47.2	–

Table 9
Central 1st principal stress values of PV panels with SSSS (unit: mPa).

Water pressure (kPa)		0	1	2	3	4	5	5.5
Test average value	Results	0	10.2	18.8	25.9	31.6	35.5	38.1
This paper	Results	0	8.5	17	25.5	34.1	42.6	46.8
	Error (%)	0	16.3	9.5	1.5	8.0	20.2	22.8
Navier method	Results	0	7.9	15.8	23.6	31.5	39.4	43.3
	Error (%)	0	22.2	15.8	8.8	0.2	11.1	13.6

deformation of PV panel with SSSS and predict its maximum deflection under ultimate load. However, due to the nonlinear deformation in test, a nonlinear elastic theory is still needed for the further study and design work.

6. Conclusions and recommendations

The aim of this paper is to study the mechanical properties of the double glass PV panel with two different boundary conditions. One of them is four edges simply supported (SSSS), and the other one is two opposite edge simply supported and the other two edges free (SSFF). Both experimental and theoretical works are completed in present paper. The researches in this paper could be a foundation to the BIPV safety study and design in future.

Based on the results we may conclude as follows:

- Hoff model, which is suitable to simulate the laminate plate with soft core, is applied in this research to describe the bending behaviour of PV panel. Two sets of boundary equations are developed based on two different boundary conditions. By using a modified Rayleigh-Rita method and a general assumption of solution, the closed form solutions are derived out and calculation programs are made for the PV panel with two boundary conditions.
- In experimental works, two boundary conditions are realized by modifying the steel frame. The water is applied to provide uniformly distributed force instead of the sand or bricks used in previous researches. And the better effects of water pressure is demonstrated by the tests.
- As stated in test data, the deformation of PV panels with SSFF is a linear elastic deformation. But it is a nonlinear elastic deformation to the PV panels with SSSS. A nonlinear elastic theory is supposed to be applied in further study for that boundary condition.
- As to the PV panel with SSFF, the calculation results from ANSYS and proposed equations are all close to the experimental results. The calculation accuracy of the proposed equations is verified by those comparisons. The deflection and stress calculated by proposed equations are even more accurate than the ones simulated by ANSYS. It is also much faster to calculate by equation (59), so it can be used in the optimal design work of BIPV component in next stage.
- As to the PV panel with SSSS, the errors between test data and calculation data are very obvious, since the ANSYS and proposed method are based on linear elastic deformation theory but the real deformation of PV panels is nonlinear. In central deflection, the results from proposed equations are very close to the ones from ANSYS and it is very accurate to calculate the maximum deflection. In central stress, proposed equations are suitable to calculate the stress when the PV panel is under small deformation, but ANSYS is better for the large deformation.
- Comparing the central deflection and central stress from different boundary conditions, the PV panels or homogenous glass panels with SSSS have much better effects. It shows that the PV panels or glass panels with SSSS can bear a larger uniformly distributed force with a smaller deformation. So it should be considered as the primary choice in the BIPV projects.
- When the four edges of PV panel are simply supported, the data from proposed method are compared with the ones from Navier method that is a classical method from laminate plate research. Both of them belong to the linear elastic deformation theory, but the data from Navier method are all smaller. The proposed method is better than Navier method in the small deformation range and predicting the maximum central deflection.
- When the water pressure is under 2.4Kpa required by current certification of PV module, there is not any damage on the surface glass. But further tests are needed to study if they can satisfy the safety requirements from the building certification for building component.
- As shown in the deflection nephogram and stress nephogram, both maximum deflection and maximum stress are located at the middle location of PV panel. It should be chosen as the key position and key point in future design work.
- The results of this paper provide a foundation for the use of PV panel as building component in BIPV. The deflection and stress results can help to make the special certification of PV panel in BIPV to ensure the safety of the component and the whole building.

Declaration

No conflict of interest exits in the submission of this manuscript, and the manuscript is approved by all authors for publication. The present work is original and has not been published previously. The manuscript will not be published elsewhere in the same form, in English or in any other language.

Acknowledgments

The authors are grateful for the financial support from the Ministry of Science and Technology of the People's Republic of China: Newton Fund - China-UK Research and Innovations Bridges (No. 2016YFE0124500).

References

[1] A Research Report of Building Energy Consumption in China, China Association of Building Energy Efficiency, 2017.
[2] Building Energy Data Book, U.S. Department of Energy, 2017.
[3] Patrina Eiffert, An Economic Assessment of Building Integrated Photovoltaics, Oxford Brookes School of Architecture, 1998.
[4] I. Ceron, E.C. Martin, F.J. Neila, 'State-of-the-art' of building integrated photovoltaic products, Renew. Energy 58 (1) (2013) 127–133.
[5] Akash Kumar Shukla, K. Sudhakar, Prashant Baredar, Recent advancement in BIPV product technologies: a review, Energy Build. 140 (1) (2017) 188–195.
[6] Emrah Biyik, Mustafa Araz, Arif Hepbasli, Mehdi Shahrestani, Running Yao, Li Shao, Emmanuel Essah, Armando C. Oliveira, Teodosio Del Cano, Elena Rico, Juan Luis Lechon, Luisa Andrade, Adelio Mendes, Yusuf Baver Atli, A key review of building integrated photovoltaic (BIPV) systems, Eng. Sci. Technol. Int. J. 20 (1) (2017) 822–858.
[7] Akash Kumar Shukla, K. Sudhakar, Prashant Baredar, A comprehensive review on design of building integrated photovoltaic system, Energy Build. 128 (1) (2016) 99–110.
[8] Bjorn Petter Jelle, Christer Breivik, Hilde Drolsum Rokenes, Building integrated photovoltaic products: a state-of-the-art review and future research opportunities, Sol. Energy Mater. Sol. Cell. 100 (1) (2012) 69–96.
[9] H.C. Curtius, The adoption of building-integrated photovoltaics: barriers and facilitators, Renew. Energy 126 (1) (2018) 783–790.
[10] D. Aelenei, R.A. Lopes, L. Aelenei, H. Goncalves, Investigating the potential for energy flexibility in an office building with a vertical BIPV and a PV roof system, Renew. Energy 137 (1) (2019) 189–197.
[11] O. Zogou, H. Stapountzis, Experimental validation of an improved concept of building integrated photovoltaic panels, Renew. Energy 36 (1) (2011) 3488–3498.
[12] M. Tripathy, S. Yadav, S.K. Panda, P.K. Sadhu, Performance of building integrated photovoltaic thermal systems for the panels installed at optimum tilt angle, Renew. Energy 113 (1) (2017) 1056–1069.
[13] L. Lu, K.M. Law, Overall energy performance of semi-transparent single-glazed photovoltaic (PV) window for a typical office in Hong Kong, Renew. Energy 49 (1) (2013) 250–254.
[14] S.A. Hosseini, A.M. Kermani, A. Arabhosseini, Experimental study of the dew formation effect on the performance of photovoltaic modules, Renew. Energy 130 (1) (2019) 352–359.
[15] A. Senturk, New method for computing single diode model parameters of photovoltaic modules, Renew. Energy 128 (1) (2018) 30–36.
[16] Changhai Peng, Ying Huang, Zhishen Wu, Building-integrated photovoltaics (BIPV) in architectural design in China, Energy Build. 43 (1) (2011) 3592–3598.
[17] IEC 61215-2005, Crystalline Silicon Terrestrial Photovoltaic (PV) Modules, International Electrotechnical Commission, 2005.
[18] Konstantin Naumenko, Victor A. Eremeyev, A layer-wise theory for laminated glass and photovoltaic panels, Compos. Struct. 112 (1) (2014) 283–291.
[19] J. Eisentrager, K. Naumenko, H. Altenbach, J. Meenen, A user-defined finite element for laminated glass panels and photovoltaic modules based on a layer-wise theory, Compos. Struct. 133 (1) (2015) 265–277.
[20] J. Eisentrager, K. Naumenko, H. Altenbach, H. Koppe, Application of the first-order shear deformation theory to the analysis of laminated glasses and photovoltaic panels, Int. J. Mech. Sci. 96–97 (2015) 163–171.
[21] Matthias Weps, Konstantin Naumenko, Holm Altenbach, Unsymmetric three-layer laminate with soft core for photovoltaic modules, Compos. Struct. 105 (1) (2013) 332–339.
[22] Stefan-H. Schulze, Matthias Pander, Konstantin Naumenko, Holm Altenbach, Analysis of laminated glass beams for photovoltaic applications, Int. J. Solids Struct. 49 (1) (2012) 2027–2036.
[23] T. Zhang, L. Xie, Y. Li, T.K. Mallick, Q. Wei, X. Hao, B. He, Experimental and theoretical research on bending behavior of photovoltaic panels with a special boundary condition, Energies 11 (12) (2018) 3435.
[24] Ajitanshu Vedrtnam, S.J. Pawar, Laminated plate theories and fracture of laminated glass plate-A review, Eng. Fract. Mech. 186 (1) (2017) 316–330.
[25] R. Szilard, Theories and Applications of Plate Analysis, John Wiley & Sons, Hoboken, New Jersey, 2004.
[26] K. Naumenko, J. Alternbach, H. Altenbach, V.K. Naumenko, Closed and approximate analytical solutions for rectangular mindlin plates, Acta Mech. 147 (1–4) (2001) 153–172.
[27] J.N. Reddy, C.M. Wang, An overview of the relationships between solutions of classical and shear deformation plate theories, Compos. Sci. Technol. 60 (12) (2000) 2327–2335.
[28] Bostjan Brank, On boundary layer in the mindlin plate model: levy plates, Thin-Walled Struct. 46 (5) (2008) 451–465.
[29] H. Altenbach, V.A. Eremeyev, Direct approach based analysis of plates composed of functionally graded materials, Arch. Appl. Mech. 78 (10) (2008) 775–794.
[30] H. Altenbach, K. Naumenko, Shear correction factors in creep-damage analysis of beams, plates and shells, JSME Int. J. Ser. A 45 (1) (2002) 77–83.
[31] C. Helfen, S. Diebels, A numerical homogenisation method for sandwich plates based on a plate theory with thickness change, ZAMM J. Appl. Math. Mech. 93 (2–3) (2013) 113–125.
[32] E. Carrera, Historical review of zig-zag theories for multi-layered plates and shells, Appl. Mech. Rev. 56 (3) (2003) 289–308.
[33] E. Carrera, S. Brischetto, P. Nali, Plates and Shells for Smart Structures: Classical and Advanced Theories for Modelling and Analysis, Wiley, 2011.
[34] E. Carrera, A. Cliuffreda, A unified formulation to assess theories of multilayered plates for various bending problems, Compos. Struct. 69 (3) (2005) 271–293.
[35] Mihir K. Pandit, Abdul H. Sheikh, Bhrigu N. Singh, An improved higher order zigzag theory for the static analysis of laminated sandwich plate with soft core, Finite Elem. Anal. Des. 44 (1) (2008) 602–610.
[36] P. Foraboschi, Analytical model for laminated glass plate, Compos. B Eng. 43 (5) (2012) 2094–2106.
[37] M. Asik, S. Tezcan, Laminated glass beams: strength factor and temperature effect, Comput. Struct. 84 (5–6) (2006) 364–373.
[38] K. Yao, E.M. Daya, Static and free vibration analysis of laminated glass beam on viscoelastic supports, Int. J. Solids Struct. 44 (25–26) (2007) 8735–8750.
[39] I.V. Ivanov, Analysis, modelling and optimization of laminated glasses as plane beam, Int. J. Solids Struct. 43 (22–23) (2006) 6887–6907.
[40] D.A. Maturi, A.J.M. Ferreira, A.M. Zenkour, D.S. Mashat, Analysis of sandwich plates with new layerwise formulation, Composites Part B 56 (1) (2014) 484–489.
[41] A.J.M. Ferreiara, C.M.C. Roque, R.M.N. Jorge, E.J. Kansa, Static deformation and vibration analysis of composite and sandwich plates using a layerwise theory and multiquadrics discretizations, Eng. Anal. Bound. Elem. 29 (1) (2005) 1104–1114.
[42] J.L. Mantari, A.S. Oktem, C. Guedes Soares, A new trigonometric shear deformation theory for isotropic, laminated composited and sandwich plates, Int. J. Solids Struct. 49 (1) (2012) 43–53.
[43] J.L. Mantari, A.S. Oktem, C. Guedes Soares, A new higher order shear deformation theory for sandwich and composite laminated plates, Composites Part B 43 (1) (2012) 1489–1499.
[44] J.L. Mantari, A.S. Oktem, C. Guedes Soares, Static and dynamic analysis of laminated composite and sandwich plates and shells by using a new higher-order shear deformation theory, Compos. Struct. 94 (1) (2011) 37–49.
[45] H. Altenbach, K. Naumenko, Creep bending of thin-walled shells and plates by consideration of finite deflections, Comput. Mech. 19 (6) (1997) 490–495.
[46] S. Kapuria, P. Kumari, Extended Kantorovich method for coupled piezoelasticity solution of piezolaminated plates showing edge effects, Proc. R. Soc. Math. Phys. Eng. Sci. 469 (469) (2013) 1–19.
[47] P. Kumari, S. Kapuria, R.K.N.D. Rajapakse, Three-dimensional extended Kantorovich solution for Levy-type rectangular laminated plates with edge effects, Compos. Struct. 107 (1) (2014) 167–176.
[48] N.J. Hoff, Bending and Buckling of Rectangular Sandwich Plates, NACA, 1950. TN2225.